Neurosafety and oncotropism of the oncolytic Farmington virus in the treatment of glioblastoma multiforme

by

Robyn Skillings

A thesis submitted in partial fulfillment of the requirements for the degree of

Master of Science in Microbiology and Immunology

Department of Biochemistry, Microbiology and Immunology

Faculty of Medicine

University of Ottawa

Supervisor Dr. David Stojdl

ABSTRACT

Glioblastoma multiforme is the most common and malignant form of brain cancer in humans. The current prognosis for glioblastoma patients undergoing standard treatment is extremely low, with a median patient survival of 1 to 2 years. Oncolytic viruses are currently being evaluated as promising novel therapies for the treatment of glioblastoma. Our laboratory's preliminary data has demonstrated that the oncolytic rhabdovirus Farmington effectively eliminates brain tumours, but is also neurosafe. However, the biological mechanisms underlying Farmington's neurosafety and oncotropism were unknown. Through studying Farmington infection in normal brain cells and brain cancer cells *in vitro*, we determined that Farmington's distinct tropism is dependent on the Farmington glycoprotein and the type 1 interferon response.

ACKNOWLEDGEMENTS

First, I would like to thank my thesis supervisor Dr. David Stojdl for providing me with the opportunity to study in his lab. My first time working in the Stojdl Lab as a summer research student was an amazing introduction to the world of research. Similarly, my Master's in the Stojdl lab helped me develop knowledge and skills that are applicable to the field of research, and to life. I am extremely grateful to Dr. Stojdl for his guidance throughout this journey and will continue to sing the praises of the Stojdl lab!

Second, I would like to thank the members of the Stojdl Lab for their guidance and support throughout my degree. My fellow Master's student Zach Jilesen has been a wonderful colleague and friend, and I greatly appreciated working on FMT alongside him. Phil Charron was a great friend as well, who helped me with a number of technical aspects of my project and spent hours developing an R script with me. Our science writer Stephanie Pontier was an exceptional mentor during my degree. She brought me onto the FMT project and helped me develop my communication and research skills immensely.

I would also like to thank all members of the Turnstone Biologics team for their assistance and friendship. I am very thankful to Charles Lefebvre for developing nearly all viruses used in my project. Charles was also a wonderful mentor during my summer research placement and my Master's, and he was always available to chat about my results. His optimistic view was always appreciated. Seb Delpeut was also a great friend and mentor during my Master's, and helped me add the proper controls to my experiments. Diwakar Bobbola always encouraged me to brave my fears, and taught me how to make authentic Indian curry.

Thank you to the members of the Alain lab. Dung Hoang was always available to help me with my experiments, and to discuss my results. His dedication to reading papers inspired me to read many papers as well, which likely saved me weeks in the lab. Nasana Vaidaya and Vickey Gilchrist were great friends and colleagues in the institute, and I could always count on them to be there on evenings and weekends.

Thank you to Skye and Chloe at the CBIA microscopy core for helping me develop my imaging experiments. They helped with many of the technical aspects of my imaging, and their advice was always appreciated. Thank you to my TAC members, Dr. Jocelyn Côté and Dr. Derrick Gibbings for their guidance and support throughout my Master's. Thank you to the members of Dr. Marceline Côté's lab for not only providing me with various reagents to test, but for helping with analysis and next steps in my experiments!

Thank you to all members of the CHEO Research Institute and the CHEO Foundation. Working for CHEO made me feel like I was part of a big family. I would especially like to thank Lynn Kyte for managing all lab orders like a boss. Thank you to Keith and David for keeping our laboratories stocked and clean as well!

And finally, thank you to my friends and family for your outstanding support. Thanks for putting up with my weird attendance at social events, and for keeping me sane these past two years. Last but certainly not least, thank you to my partner Nick Burns for being my best friend and for being supportive no matter what.

Table of Contents

LIST OF ABBREVIATIONS

Au	Arbitrary unit
BBB	Blood brain barrier
cDNA	Complementary deoxyribonucleic acid
CNS	Central nervous system
DAMP	Damage-associated molecular pattern
DIC	Differential interference contrast
DiD	1,1′-dioctactadecyl-3,3,3′,3′-tetramethylindodicarbocyanine
DiD-FMT	Farmington virus labeled with DiD
DiD-FMT-(MRB-G)	Farmington virus encoding the Maraba glycoprotein labeled with DiD
DMEM	Dulbecco's Modified Eagle Medium
DNA	Deoxyribonucleic acid
EEA1	Early endosome associated protein 1
eGFP	Enhanced green fluorescent protein
ELISA	Enzyme-linked immunosorbent assay
FBS	Fetal bovine serum
FMT	Farmington virus
FMT-(MRB-G)	Farmington virus encoding the Maraba glycoprotein
FMT-(MRB-G)-eGFP	Farmington virus encoding the Maraba glycoprotein and enhanced green fluorescent protein
FMT-eGFP	Farmington virus encoding enhanced green fluorescent protein
GBM	Glioblastoma multiforme
GFP	Green fluorescent protein
eGFP	Enhanced green fluorescent protein
IC	Intracranial
IFITM	Interferon-induced transmembrane proteins
IFN	Interferon
IFNAR	Interferon-alpha/beta receptor
Ifnb1	Interferon beta 1 mRNA
IFNβ1	Interferon beta 1 protein
IgG	Immunoglobulin antibody
ISG	Interferon-stimulated gene
JAK-STAT	Janus kinase signal transducer and activator of transcription
LAMP1	Lysosomal-associated membrane protein 1
LASV	Lassa virus
LCMV	Lymphocytic choriomeningitis virus

LDLR	Low density lipoprotein receptor
MOI	Multiplicity of infection
MRB	Maraba virus
MRB MG1	Maraba MG1 virus
MRB-(FMT-G)	Maraba virus encoding the Farmington glycoprotein
MRB-eGFP	Maraba virus encoding enhanced green fluorescent protein
mRNA	Messenger RNA
NH4Cl	Ammonium chloride
NHA	Normal human astrocytes
OV	Oncolytic virus
PAMP	Pathogen-associated molecular pattern
PBS	Phosphate buffered saline
PCR	Polymerase chain reaction
Pfu	Plaque forming unit
PRR	Pattern recognition receptor
qPCR	Quantitative polymerase chain reaction
RFP	Red fluorescent protein
RIG-1	Retinoic-acid-inducible gene 1
RNA	Ribonucleic acid
RPM	Rotations per minute
ssRNA	Single-stranded ribonucleic acid
TLR4	Toll-like receptor 4
TLR7	Toll-like receptor 7
VACV-eGFP	Vaccinia virus encoding enhanced green fluorescent protein
VACV	Vaccinia virus
VLP	Virus-like particle
VSV	Vesicular stomatitis virus
VSV-eGFP	Vesicular stomatitis virus encoding enhanced green fluorescent protein
VSVΔ51	Vesicular stomatitis virus with a deletion in methionine at position 51 within the genome
VSVΔ51-eGFP	Vesicular stomatitis virus with a deletion in methionine at position 51 within the genome encoding enhanced green fluorescent protein

LIST OF FIGURES

1. INTRODUCTION

Cancer is one of the leading causes of death prior to age 70 in 91 countries worldwide, and its incidence and mortality continue to grow internationally [1]. Current standard-of-care therapies for cancer include chemotherapy, radiotherapy, and surgical resection of the tumour [2]. However, efficacy remains low due to resistance to treatment, cancer recurrence, and/or negative side effects [3–5]. Therefore, novel approaches to treating cancer are greatly needed.

1.1 Oncolytic virotherapy

One such approach is oncolytic virotherapy. Oncolytic viruses (OVs) are replication-competent viruses that selectively replicate in tumour cells, leading to tumour cell lysis and the release of viral progeny [6]. Viral progeny then infects neighbouring tumour cells, continuing the infection and destruction of the tumour. This self-amplifying quality is unique to OV therapy and allows for the application of lower viral doses [7]. In addition to direct tumour cell lysis, OVs have an immunogenic effect on tumours as well. Upon viral-mediated cell death, tumour associated antigens and damage-associated molecular patterns (DAMPs) are released, which prime and activate anti-tumour immunity [8–11]. Additionally, viral infection of tumours can reshape the tumour microenvironment, reversing immunosuppression and promoting anti-tumour immunity [12–14]. As the selectivity of OVs for tumour cells relative to normal cells dictates much of the efficacy and safety of these therapies, viral tropism remains a key area of research in the field of oncolytic virotherapy [15,16]. This tropism is dictated by a number of virus-host interactions, including antiviral mechanisms in normal cells and mechanisms of susceptibility within cancer cells.

1.2 Virus-host interactions governing the tropism of oncolytic viruses

1.2.1 The type 1 interferon response

One of the major virus-host interactions governing OV tropism is the type 1 interferon (IFN) response. The type 1 IFN response is an innate antiviral response that inhibits viral infection within normal cells [17]. During viral infection, cellular pattern recognition receptors (PRRs) recognize pathogen-associated molecular patterns (PAMPs) in viral proteins and viral genomic material [18,19]. These interactions activate PRR-dependent signaling cascades that result in the production of antiviral cytokines known as IFNs. In an autocrine and paracrine fashion, IFNs bind to the interferon-alpha/beta receptor (IFNAR) and induce a signaling cascade through the Janus kinase signal transducer and activator of transcription (JAK-STAT) [20,21]. This signaling then activates the expression of IFN-stimulated genes (ISGs). ISGs restrict all stages of the viral replication cycle in infected and neighbouring uninfected cells, [22,23], thus protecting normal cells from OV infection.

In contrast to normal cells, tumour cells often have dysregulated or dysfunctional IFN signaling pathways [24–26], making them susceptible to OV infection. As IFNs can suppress tumour growth, cancer cells often develop mutations within their IFN signaling cascades to enhance tumour proliferation [27]. Mutations can be present at all levels of the IFN response, from mutations within PRRs, the JAK-STAT pathway, ISGs, or the IFNAR [28,29]. The differential in the functionality of the type 1 IFN response between normal cells and cancer cells is a key factor underlying OV tropism.

1.2.2 Viral entry

In addition to the antiviral response, viral entry is a key process that governs the selectivity of OVs as well. The first stage of viral entry that influences OV tropism is viral attachment to the host cell surface [30]. Viral attachment is primarily mediated through interactions between cell surface receptors and viral glycoproteins embedded in the viral membrane [31]. The success of these interactions is governed by the expression of viral entry receptors on the cell surface, as well as the affinity of the glycoprotein-receptor interaction. High expression levels of an OV's specific viral entry receptor on the cell surface can increase viral selectivity for that cell type. Several OVs inherently attach to receptors that are upregulated in cancer cells, thus improving their selectivity for tumour cells. For example, the oncolytic herpes simplex virus known as T-VEC uses the receptors HVEM, nectin-1, and nectin-2 to enter cells [32]. The expression of these receptors is upregulated in cancer cells relative to normal cells, thus increasing the tropism of T-VEC for tumour cells. Viral tropism is also influenced by the affinity of an OV's glycoprotein to its viral entry receptor. Higher affinity glycoprotein-receptor interactions often correlate with better infectivity. In one study, a panel of measles viruses with different binding affinities to the HER2 receptor were generated for treatment of HER2/neu-expressing tumours [33]. The viruses with binding affinities to the HER2 receptor that were above a minimum threshold infected the tumour cells efficiently, whereas viruses with binding affinities below this threshold showed minimal infection. Altogether, these studies demonstrate that viral attachment is an important factor influencing OV tropism.

For enveloped viruses, fusion of the viral envelope with a host membrane is a key step dictating viral tropism as well. Interferon-induced transmembrane proteins (IFITMs) are a family of ISGs that restrict the viral fusion of numerous viruses within normal cells [34]. While the expression of these proteins increases upon IFN signaling, basal levels of these proteins are sufficient to block viral entry in normal cells [34–36]. The IFITM2 and IFITM3 proteins specifically restrict viral fusion in endosomes and lysosomes by inhibiting pore formation [37], shuttling viruses to lysosomes for degradation [38], or disrupting endosomal cholesterol homeostasis [39]. Viral fusion can also be restricted in the absence of specific host factors required to complete this process. For example, Lassa virus (LASV) uses the lysosomal-associated membrane protein 1 (LAMP1) as its intracellular receptor [40]. However, LASV viral fusion is restricted in bird cells due to the absence of a glycosylated residue in LAMP1 required for this interaction [41]. Thus, different sequences or glycosylation patterns in receptors required for viral fusion can affect selectivity as well.

1.3 OV treatment of glioblastoma multiforme

OV tropism is particularly important in the treatment of glioblastoma multiforme. Glioblastoma multiforme (GBM) is the most common and malignant form of brain cancer in humans [42]. Despite improvements in chemotherapy, radiation, and surgery, the current prognosis for GBM patients undergoing treatment is approximately 1 to 2 years [43]. It has been argued that OV treatments for GBM should be delivered intracranially (IC) to allow direct access to the brain tumour to have the highest oncolytic effect [7,44,45]. However, IC injection of an OV increases the risk for infection within the brain. Two primary brain cell populations at risk for infection are neurons and astrocytes. Neurons are arguably the most functionally important cells within the brain as neural circuitry is responsible for brain

function [46]. Neurons are also non-renewable cells [47]; therefore, virus-mediated cell death in neurons can permanently damage neural circuitry [48]. Astrocytes are glial cells that support neuronal function, blood brain barrier integrity, and provide homeostasis within the brain [49]. Virus-mediated cell death within astrocytes can lead to loss of blood brain barrier integrity, neuronal damage, and dysregulated signaling within the brain [50]. Infection within the brain can also damage normal brain tissues indirectly through inflammation. Immune cell infiltration and proinflammatory cytokines produced in response to infection within the brain can damage normal brain tissues [51,52]. Direct or indirect damage to either astrocytes or neurons can have severe neurological consequences, including encephalitis, decreased motor and sensory functions, and even death [48,53]. It is critical that OV infection is strictly attenuated within normal brain tissues in the treatment of GBM. Therefore, understanding the virus-host interactions governing tropism for normal brain tissues is essential to improving the safety of these therapies.

In addition to safety concerns, OV selectivity for brain tumour cells can impact the efficacy of these therapies as well. Due to the heterogeneity of GBM tumours, several gliomas are very susceptible to OV infection and therefore demonstrate high efficacy in GBM mouse models [54–56]. However, other GBM tumours can restrict infection, thus reducing efficacy [57,58]. One mechanism that dictates glioma susceptibility to OV infection is the presence of IFN signaling within the tumour, where gliomas with intact IFN responses can restrict OV replication [59]. However, the mechanisms underlying the efficacy of OV therapies for treating GBM remain elusive as well. Therefore, studying the mechanisms governing OV selectivity for brain cancer cells could improve the efficacy of these GBM therapies.

1.4 Oncolytic rhabdoviruses for treating GBM

One group of viruses being considered for the treatment of GBM is the *Rhabdoviridae* family. Rhabdoviruses possess many qualities of an ideal OV, including high oncolysis, rapid replication cycles, broad cell tropism, high virus yields, low serology in humans, and flexible genomic platforms for transgene insertion [60]. One such rhabdovirus is the vesicular stomatitis virus (VSV), a member of the *vesiculovirus* genus. VSV is a rhabdovirus with a negative sense, single-stranded ribonucleic acid (ssRNA) genome. This virus was discovered to be highly oncolytic towards many cancers, and its sensitivity to IFN made it safe for normal tissues [26].

The discovery of VSV prompted the search for other rhabdoviruses with similar oncolytic properties. From this search, a close relative of VSV that also belonged to the *vesiculovirus* genus was discovered. Maraba virus (MRB) was lytic against 100% of the 37 cancer cell lines tested, and was also IFN sensitive [60]. Despite the IFN sensitivity of these two viruses, it was discovered that wildtype VSV infected tissues of the central nervous system (CNS) and the brain within rodents and nonhuman primates, making it neurotoxic [61–63]. It was therefore assumed that wildtype MRB would be similarly neurotoxic. Unfortunately, this inhibited the use of wildtype VSV and MRB as OVs at therapeutic doses.

In an attempt to increase the safety of MRB and VSV, attenuated versions of these two viruses were created, known as MRB MG1 and VSVΔ51, respectively. The mutations in these viruses inhibited their ability to block host gene expression and IFN signaling within normal tissues. This increased the IFN sensitivity of these viruses and improved their safety [64–67]. MRB MG1 is currently in two clinical trials for treating cancer [68] and

VSVΔ51 is in preclinical stages of development [69–71]. Despite the attenuated nature of these viruses in tissues outside the brain, administration of maximum doses of MRB MG1 or VSVΔ51 by intravenous injection results in infection of CNS tissues, including within the brain [55,60,72]. This diminished the possibility of using these viruses for IC treatment of GBM. However, it also highlighted that while important, the IFN response alone cannot protect against OV infection within the brain.

In addition to the IFN response, it was later appreciated that the viral glycoprotein was a key determinant for neurotropism as well. For example, it was discovered that the VSV glycoprotein mediates this virus' neurotropism, as it uses the widely-expressed low density lipoprotein receptor (LDLR) as its viral entry receptor [73]. To improve VSV's neurosafety for the treatment of GBM, VSV pseudotypes were developed where the VSV glycoprotein was removed and replaced with a non-neurotropic glycoprotein [61,74,75]. One study engineered a VSV variant pseudotyped with the Lassa virus glycoprotein precursor (LASV-GPC), known as VSV-LASV-GPC [76]. This virus demonstrated attenuated infection within brain cells. As well, no neurotoxicity was observed within mice and the treatment was capable of prolonging survival in xenograft mouse models of glioblastoma. Similarly, a VSV variant pseudotyped with the lymphocytic choriomeningitis virus glycoprotein (LCMV-GP) known as rVSV(GP) demonstrated minimal infection within brain cells. This virus demonstrated little to no adverse effects within the brain, and the treatment prolonged survival in both syngeneic and xenograft mouse models of glioblastoma [77]. Interestingly, the LCMV glycoprotein is known to use α-dystroglycan, a protein expressed on the cell surface of numerous brain cell populations, as its entry receptor [78,79]. However, α-dystroglycan may have different

glycosylation patterns or expression levels in normal brain cells compared to brain cancer cells [80,81]. As well, the absence of a coreceptor required for entry into normal brain cells could restrict this virus, as has been demonstrated with different OVs [82]. Altogether, these studies emphasize the importance of the viral glycoprotein in dictating neurotropism. However, the glycoprotein-dependent mechanisms underlying neuroattenuation remain elusive for many OVs.

1.5 Farmington virus

One oncolytic rhabdovirus with elusive mechanisms of selectivity is the Farmington virus (FMT). FMT was identified alongside MRB in the screen for novel rhabdoviruses with highly oncolytic properties [60]. Like MRB and VSV, FMT was a rhabdovirus that was highly lytic against multiple cancer cell lines, with a particular tropism for tumours from the CNS. However, unlike MRB and VSV, the sequence of the FMT polymerase (L protein) was more closely related to the plant-tropic genus *cytorhabdovirus* [83]. Interestingly, wildtype FMT could be injected intracranially or intravenously into mice at high titres without neurotoxicity, making it neurosafe (unpublished data). Together, FMT's oncotropism and unique neurosafety profile confirmed its potential as an OV for the treatment of GBM.

Since its discovery in 2010, our laboratory has developed FMT as a novel OV platform for treating GBM. We have demonstrated that IC delivery of FMT eliminates brain tumours in both xenograft and syngeneic mouse models of glioblastoma, generating long-lasting cures. Recently, IC injection of FMT in nonhuman primates was found to be well tolerated in the brain with no observed toxicity (unpublished data). FMT is therefore on its way to a clinical trial for the treatment of GBM in human patients. However, the

mechanisms underlying FMT's unique neurosafe and oncotropic properties have not been explored.

1.6 Rationale and hypothesis

Multiple studies have correlated viral neurosafety with restricted infection within the brain [61,74–77]. Our own studies suggested that this correlation may pertain to FMT as well. Immunostaining of mouse brain sections 48 hours after IC administration of FMT revealed only limited FMT staining within brain tissues. In contrast, extensive staining was observed with VSV treatment in various regions of the brain. Therefore, we predicted that FMT's neurosafety may partially depend on an attenuated capacity to infect normal brain cells. However, FMT's capacity to infect normal brain cells had not been characterized *in vitro.* As our preliminary data suggested that FMT's infection in normal brain cells was attenuated, we predicted that this attenuation would depend on two major factors: the type 1 IFN response and the FMT glycoprotein. As the IFN response is a key antiviral mechanism for many OVs [22,23], we predicted that the IFN response would be an important factor governing FMT's neurosafety as well. Our preliminary data suggested that FMT induced IFN signaling within normal human fibroblasts, to which FMT's replication cycle is sensitive. As well, IFNAR-/- knockout fibroblasts are susceptible to FMT infection. Therefore, we suspected that the type 1 IFN response may similarly restrict FMT infection within normal brain cells.

We also suspected that the FMT glycoprotein played a role in FMT's neurosafety as well. This hypothesis is based on *in vivo* studies with FMT pseudotypes. For example, IC injection of a FMT variant pseudotyped with the MRB glycoprotein (FMT-(MRB-G)) caused neurotoxicity in mice. In contrast, IC injection of a MRB variant pseudotyped with

the FMT glycoprotein (MRB-(FMT-G)) was neurosafe. This paralleled the neurotropism studies of VSV variants pseudotyped with the LCMV or LASV glycoproteins [76,77]. These studies suggested that the MRB glycoprotein was neurotropic, whereas the FMT glycoprotein was not. As viral entry is a glycoprotein-mediated step in the viral replication cycle [31], FMT viral entry could be restricted in normal brain cells relative to entry mediated by the MRB glycoprotein. In contrast, our preliminary data demonstrated that FMT and MRB were very oncotropic towards tumours from CNS origins. This suggested that viral entry mediated by the FMT glycoprotein may proceed more efficiently within brain cancer cells, and perhaps at similar levels to the MRB glycoprotein.

Therefore, we hypothesize that FMT's balance of oncotropism and neurosafety is dependent on its distinct tropism for brain tumour cells relative to normal brain cells, which is influenced by the IFN response and the FMT glycoprotein.

Our first objective was to determine FMT's neurovirulence *in vitro.* As seen with other neurosafe viruses [76,77], we expected that FMT would minimally infect neurons. We explored the neurovirulence of the neurotoxic viruses MRB, FMT-(MRB-G), VSV, and VSVΔ51 as well. As previously established in the literature, we expected that VSV and VSVΔ51 would infect neurons. MRB's neurotoxicity has been characterized *in vivo*; therefore, we predicted that MRB would be neurotropic *in vitro*. As FMT-(MRB-G) also uses the MRB glycoprotein, we expected this virus to be neurovirulent well. Altogether, we sought to establish a correlation between viral neurotoxicity and neurotropism, as previously described. As well, we hoped these experiments would highlight the influence of the viral glycoprotein in neurotropism.

As an important antiviral mechanism dictating the safety of many oncolytic viruses, our second objective was to determine if FMT induced type 1 IFN expression which then restricted FMT infection in normal brain cells. IFN beta is often one of the earliest type 1 interferons produced during viral infection, and is a key player in the IFN response [84–86]. IFN is produced by both neurons and astrocytes, with astrocytes acting as a primary producer of IFN beta [87]. We therefore evaluated FMT's capacity to induce IFN beta expression within astrocytes. As seen in fibroblasts, we expected FMT to induce IFN beta expression within astrocytes at high levels. As neurons produce IFN beta, we evaluated if FMT infection was restricted by IFN beta signaling in neurons as well. We also investigated a potential link between the IFN response and the viral glycoprotein in FMT's neurosafety. Studies have found that certain viral glycoproteins can induce IFN signaling through interactions with PRRs such as toll-like receptor 4 (TLR4) [88–90]. Therefore, we compared IFN expression in astrocytes infected with FMT and FMT-(MRB-G) to test if IFN induction was glycoprotein-dependent.

Our third and final objective was to evaluate the role of the viral glycoprotein in dictating FMT's tropism in brain cancer cells relative to normal brain cells. As viral entry is a glycoprotein-dependent step [31], we suspected that FMT viral entry may be attenuated within normal brain cells compared to brain cancer cells. As well, we suspected that viral entry mediated by the FMT glycoprotein may proceed at similar efficiencies to the MRB glycoprotein. We therefore chose to compare the viral entry of FMT and FMT-(MRB-G) in astrocytes and the glioblastoma cell line U343. To exclude the possibility that the glycoprotein affected a post-entry stage of the viral replication cycle, we evaluated the viral transcript abundance of FMT and FMT-(MRB-G) in

astrocytes and U343 cells. Next, we studied the levels of viral attachment, viral fusion, and the pathway of viral entry of FMT and FMT-(MRB-G) in astrocytes and U343 cells. Altogether, the main aim of this study was to determine the mechanisms underlying FMT's unique neurosafe and oncotropic profile.

2. MATERIALS AND METHODS

2.1 Cell lines

Vero and U343 cells were purchased from ATCC and maintained in 1X Dulbecco's Modified Eagle Medium (DMEM; Thermo Fisher) supplemented with 10% fetal bovine serum (FBS; Corning) at 37ºC and 5% CO_2. Cells were maintained in 15 cm tissue culture plates (Corning) until reaching approximately 70% confluence. For passaging, media was removed by aspiration and cells were washed once with phosphate buffered saline (PBS). Cells were incubated with 0.25% trypsin until lifted off (approximately 5 minutes), then resuspended in complete media. An appropriate amount of resuspended cell solution was added to a new 15 cm plate containing complete media.

Normal human astrocytes (NHA) were purchased from Lonza and cultured in Astrocyte Media (ScienCell) supplemented with 2% FBS, Astrocyte Growth Supplement, and 1% penicillin/streptomycin solution (ScienCell). Astrocytes were maintained in T25 cell culture flasks (Corning) until reaching approximately 50% confluence. For passaging, media was removed by aspiration and cells were washed once with PBS. Cells were incubated with 1X Versene (Gibco) until lifted off (approximately 10 minutes), then resuspended in complete media. Cells were pelleted

by centrifugation at 900 rotations per minute (RPM) for 5 minutes. Cell pellets were resuspended in complete media and an appropriate volume was transferred to a new flask containing complete media.

Neuronal and blood brain barrier endothelial cell cultures were kindly extracted and cultured by Dr. Sarah Schock at the CHEO Research Institute II, Ottawa, Canada. Primary culture neurons from the hippocampus, cortex, and striatum, as well as endothelial cells from the blood brain barrier were extracted from the brains of CD-1 mice (Charles River). Neurons and endothelial cells were seeded at 8E4 cells/well in 96-well plates. Neuronal cultures were maintained in B-27 supplemented Neurobasal Medium (Invitrogen) for 2 weeks before infection. Endothelial cultures were maintained in Endothelial Cell Medium (ScienCell) and were infected 3-4 days after seeding.

2.2 Viruses

All rhabdoviral stocks, including FMT-eGFP, FMT-(MRB-G)-eGFP, MRB-eGFP, VSV-eGFP, and VSVΔ51-eGFP, were kindly cloned and generated by Charles Lefebvre and Melanie Labelle at the CHEO Research Institute II, Ottawa, Canada. Vero cells were grown in 15 cm plates to 100% confluency. Cells were infected with sucrose cushion-purified viruses at MOI 0.01 in complete media at 37ºC for either 20 hours (MRB and VSV viruses) or 30 hours (FMT viruses). Media was collected and centrifuged to pellet cells. Supernatant was filtered using 0.22 µm Corning bottle-top vacuum filter systems (Sigma). Viruses were pelleted by centrifugation at 10 000 rotations per minute (rpm) for 2 hours at 4ºC. Viral pellets were resuspended in Solution C and incubated overnight at 4ºC. The following day, a 15-35% Opti-Prep gradient was prepared using a Gradient Master 108 (Biocomp Instruments). Virus was

added to the gradient, then the solution was centrifuged at 36 000 rpm for 1.5 hours at 4ºC. The virus band was collected, aliquoted, and stored at -80ºC.

The VACV-eGFP virus was kindly generated by Kristina Allan at the CHEO Research Institute II, Ottawa, Canada. U2OS cells were grown in 15 cm plates to 100% confluency. Cells were infected with sucrose-purified virus at MOI 0.1 in complete media at 37ºC for approximately 60 hours until sufficient cytopathic effect is observed. Cells were scraped off plates and resuspended by pipetting up and down vigorously. The cell solution was centrifuged at 2000 g for 10 minutes to pellet cells. The supernatant was discarded, and the pellet was resuspended in 1 mM Tris pH 9.0. The suspension was frozen overnight at -80ºC. The next day, the suspension was subjected to three freeze-thaw cycles, where the suspension was thawed in a 37ºC water bath for 15 minutes, vortexed, then frozen again at -80ºC for 30 minutes. The suspension was then centrifuged at 2000 g for 10 minutes; the supernatant containing the virus was aliquoted and stored at -80ºC.

2.3 Plaque assay

Vero cells were seeded in 6-well plates at 6E5 cells/well. The following day, cells were infected with serially diluted virus for 1 hour. Agarose overlay containing a 1:1 mixture of 1% agarose and 2X DMEM with 20% FBS was added at 2 ml/well. Plaques were counted 48 hours post-infection by eye.

2.4 Primary culture mouse neuron infection assay

Primary neuronal and endothelial cultures were cultured in 96-well plates, then infected with FMT-eGFP, FMT-(MRB-G)-eGFP, MRB-eGFP, VSV-eGFP, or VSVΔ51-eGFP at MOI 0.1 and 1. Cells were imaged in real time using the IncuCyte live cell

imaging system (Sartorius). Four images per well were taken every two hours for a total of 30 hours with the phase contrast and GFP channels. 2 biological replicates of this experiment were performed with three technical replicates per sample. Representative images and total green object area per well values were analyzed using IncuCyte ZOOM software (Sartorius). Prism 8 software (GraphPad) was used to plot the mean and standard deviation of GFP area over time and at 20 hours post-infection for the different samples. Prism was used to perform a one-way ANOVA with a Dunnett's post hoc test for multiple comparisons of the uninfected control GFP levels to all virus samples. ns = non-significant.

2.5 Time-course qPCR in NHA and U343 cells

Cell seeding and infection

NHA and U343 cells were seeded at 1.5E4 and 3E4 cells/well, respectively, into 96-well plates one day prior to infection. Cells were incubated with either FMT-eGFP, FMT-(MRB-G)-eGFP, or PBS diluted in complete media at MOI 5 with three technical replicates per sample.

Imaging

One plate of infected cells was imaged in real time using IncuCyte live cell imaging, with four images taken per well in the GFP and phase contrast channel every 2 hours for a total of 24 hours. Representative images and total green object area per well values were analyzed using IncuCyte ZOOM software (Sartorius). Prism 8 software (GraphPad) was used to plot the mean and standard deviation of GFP area over time. Prism was used to perform a two-way ANOVA with a Tukey's post hoc test for multiple

comparisons of the uninfected control to all virus samples, or comparing FMT-eGFP to FMT-(MRB-G)-eGFP. ns = non-significant, * = significant, *** = very significant.

qPCR

In a parallel experiment, cells were incubated with virus for 0, 1, 2, 4, 8, 16, or 24 hours at 37ºC. After the allotted incubation time, cells were lysed with 100 µl of RLT buffer (Qiagen). Total RNA was extracted from infected cells using the 96 RNeasy kit (Qiagen), as per the manufacturer's instructions. RNA concentration was measured using a BioTek plate reader to confirm extraction efficiency (data not shown). 10 ng of RNA was reverse transcribed using either a FMT nucleoprotein mRNA-specific primer containing a random sequence tag at its 5' end (5'- GGCAGTATC GTGAATTCGATGCTTTTTTTTTTTTTTTTTTTGTTAA-3') or an oligo(dT)18 primer (Thermo Fisher). Complementary deoxyribonucleic acid (cDNA) was amplified by Real-Time PCR; amplicons were detected using the SYBR® Green (Qiagen) fluorescent reporter on the CFX96 Touch Real-Time PCR Detection System (BioRad). FMT N mRNA-specific forward primers (5'- TAAGCTTCACTGCCGGTAGTTTAGG-3') and tag-specific primers (5'-GGCAGTATCGTGAATTCGATGC-3') were used to amplify FMT N mRNA cDNA. The Hs_GAPDH_2_SG_QuantiTect Primer Assay (Qiagen) was used to amplify *Gapdh* mRNA from the oligo(dT)18 samples. The Hs_IFNB1_1_SG_QuantiTect Primer Assay was used to amplify *Ifnb1* mRNA from the oligo(dT)18 samples. Raw C_t values were identified using the CFX Maestro (BioRad) software. ΔC_t values were calculated by subtracting the FMT N or *Ifnb1* mRNA C_t values from the *Gapdh* mRNA C_t values. The $\Delta\Delta C_t$ values (relative mRNA abundance) were calculated using the equation $2^{\Delta Ct}$. Prism 8 software (GraphPad) was used to plot the mean and standard

deviation of the relative mRNA transcript abundance over time. Prism was used to perform a two-way ANOVA with a Tukey's post hoc test for multiple comparisons of the uninfected control transcript abundance to all virus samples, or comparing FMT-eGFP versus FMT-(MRB-G)-eGFP. ns = non-significant, *** = very significant, ** = very significant.

2.6 IFNβ1 ELISA in NHA cells

NHA cells were seeded in 96-well plates at 1.5E4 cells/well the day before infection. Astrocytes were infected with FMT-eGFP, FMT-(MRB-G)-eGFP, or MRB-eGFP at MOI 5, and incubated at 37ºC. After 24 hours post-infection, supernatants were collected and IFNβ1 concentration was analyzed with a 96-well human IFN-beta ELISA kit (Biotechne), as per the manufacturer's instructions. 2 biological replicates of this experiment were performed with two technical replicates per sample. Prism 8 software (GraphPad) was used to plot the mean and standard deviation of the IFNβ1 concentration. Prism was used to perform a one-way ANOVA with a Tukey's post hoc test for multiple comparisons of the different samples. *** = very significant, ### = very significant, ns = non-significant.

2.7 IFNβ1-Neutralization in mouse cortical neurons

Mouse cortical neurons were seeded as previously described. Cells were infected with FMT-eGFP or MRB-eGFP at MOI 0.1 in triplicate for 1 hour. After 1 hour, mouse IFNβ1-neutralizing antibodies (Biotechne) or control IgG antibodies from mouse serum (Sigma) were added at different concentrations. Infected cells were imaged in real time using IncuCyte life cell imaging, with four images taken per well in the GFP and phase contrast channels every 2 hours for a total of 60 hours. Representative

images and total green object area per well values were analyzed using IncuCyte ZOOM software (Sartorius). Prism 8 software (GraphPad) was used to plot the mean and standard deviation of GFP area over time, as well as the GFP area at 24 hours post-infection. Prism was used to perform an unpaired t test, comparing GFP levels from infected neurons in the presence of IFNβ1-neutralizing antibodies versus control IgG antibodies. ns = not significant, ** = very significant.

2.8 Viral attachment assay

Seeding and infection

NHA and U343 cells were seeded at 1.5E4 and 3E4 cells/well into 96-well plates the day before infection. Cells were washed with ice-cold PBS three times, then bound with FMT-eGFP, FMT-(MRB-G)-eGFP, or PBS at MOI 10 for 1 hour at 4ºC in triplicate. Cells were washed with ice-cold PBS three times to remove unbound virions, then lysed with RLT buffer (Qiagen). Total RNA was extracted as previously described.

qPCR

A multiplex qPCR reaction with primers and fluorescent probes (IDT) were used to amplify *Gapdh* mRNA and FMT-eGFP and FMT-(MRB-G)-eGFP viral genomes. The primer-probe set for the FMT-eGFP and FMT-(MRB-G)-eGFP viral genomes was designed to span a 155 bp region across the phosphoprotein and matrix protein sequences of the FMT genome using Geneious software (BioMatters). The sequences were 5’-AGCGCTGCAGATCTTCACCAC-3’ (forward), 5’-ACCGACGCATAACGACCGTATC-3’ (reverse), and 5’-/5HEX/TAGCCTAAC/ZEN/TCACGAACGTTCCTCTC/3IABkFQ/-3’ (probe). The *Gapdh* primer and probe sequences were 5’-TGTAGTTGAGGTCAATGAAGGG-3’ (forward),

5’-ACATCGCTCAGACACCATG-3’ (reverse), and 5’-/56-FAM/AAGGTCGGA/ZEN/GTCAACGGATTTGGTC/3IABkFQ/-3’ (probe). 100 ng of RNA was amplified using a TaqMan RNA-to-Ct 1-Step Kit (Thermo Fisher) on the CFX96 Touch Real-Time PCR Detection System (BioRad). C_t values were calculated as previously described. Prism 8 software (GraphPad) was used to plot the mean and standard deviation of the relative RNA abundance. Prism was used to perform an unpaired t test comparing the relative RNA abundance of FMT-eGFP versus FMT-(MRB-G)-eGFP. ** = very significant, * = significant.

Confocal imaging

U343 cells were seeded on coverslips the day prior to infection at 3E8 cells/coverslip. To improve adherence of NHA cells, coverslips were pre-treated with rat tail collagen 1 (Corning) for 1 hour. Three days prior to infection, coverslips were washed three times in PBS, then NHA cells were seeded at 3E4 cells/coverslip. Cells were bound with FMT-eGFP, FMT-(MRB-G)-eGFP or PBS at MOI 50 for 1 hour at 4ºC. Cells were washed with ice-cold PBS three times. Coverslips were fixed and stained with anti-FMT antibody before mounting with DAPI-fluoromount (Southern Biotech). Single-slice images were taken at 60X magnification in the DAPI and FITC channels with an Olympus FV-1000 confocal microscope. The laser settings for the DAPI and FITC channels were HV 490 V, 1X gain, 5% offset, 10% laser intensity and HV 450 V, 1X gain, 5% offset, and 1% laser intensity, respectively. Brightness in the FITC channel was adjusted equally in ImageJ (NIH) among the different images to allow visualization of viral puncta.

Titration

Viral stocks were titred via plaque or via qPCR. For the qPCR method, viral RNA was extracted using the Viral RNA Isolation Kit (Qiagen) by Matteo Da Ros from Turnstone Biologics. qPCR of the viral genomes was performed by Phil Charron using the FMT genome-specific primers. Ct values were compared to a standard curve to determine the quantity of viral genome present. Prism 8 software (GraphPad) was used to plot the mean and standard deviation of the viral titres. Prism was used to perform an unpaired t test comparing the titres determined by qPCR versus plaque assay. Ns = non-significant.

2.9 Endosome acidification drug inhibitors

U343 cells were seeded into 96-well plates at 3E4 cells/well one day prior to infection. Cells were incubated with endosomal acidification drug inhibitors bafilomycin B1 (Cayman Chemicals), chloroquine diphosphate (BioTechne), or ammonium chloride (Sigma) for 1 hour at 37ºC. MRB-eGFP, FMT-(MRB-G)-eGFP, FMT-eGFP, VSV-eGFP, or VACV-eGFP at MOI 0.1 was added. Cells were imaged in real time using IncuCyte live cell imaging, with four images taken per well in the GFP and phase contrast channels every 2 hours for a total of 40 hours. Representative images and total green object area per well values were analyzed using IncuCyte ZOOM software (Sartorius). In a parallel experiment, cells were incubated with drug, then YOYO-3 reagent was added at 200 nM to monitor drug-induced cytotoxicity. Cells were imaged in the red fluorescent protein (RFP) and phase contrast channels using the IncuCyte system as in the parallel experiment. Prism 8 software (GraphPad) was used to plot the mean and standard deviation of GFP or RFP area over time, as well as the GFP or RFP area at 14 and 20 hours post-infection, respectively. Prism was used to perform a one-way

ANOVA, comparing GFP levels from infected cells with no drug compared to cells with the highest drug concentration. *** = very significant, * = significant.

2.10 Indirect DiD-labeling of FMT and FMT-(MRB-G)

Vero cells were grown in 15 cm plates to over-confluence. Cells were incubated with 25 μM lipophilic dye 1,1′-dioctactadecyl-3,3,3′,3′-tetramethylindodicarbocyanine (DiD, Thermo Fisher) diluted in 20 ml complete media for 18 hours. Labeled plates of cells were washed three times with PBS, then infected with FMT, FMT-(MRB-G), or PBS at MOI 3 diluted in 15 ml serum- and phenol-free DMEM (Gibco). When the majority of cells were rounded (about 16-20 hours post-infection), media containing viral particles was collected and filtered through a 0.22 μm Corning bottle-top vacuum filter system (Sigma). Media stocks were titred using the plaque assay method.

2.11 Imaging of DiD-labeled viruses

Confocal

To confirm labeling, U343 cells seeded on coverslips were bound with DiD-labeled FMT, FMT-(MRB-G) or PBS at MOI 50 for 1 hour at 4ºC. Cells were washed with ice-cold PBS three times. Coverslips were fixed and mounted with DAPI-fluoromount (Southern Biotech). Single-slice images of each sample were taken at 60X magnification in the DAPI and Alexa Fluor-647 channels with an Olympus FV-1000 confocal microscope. Brightness in the Alexa Fluor-647 channel was adjusted equally among the different images in ImageJ (NIH) to allow visualization of viral puncta.

High MOI infection in astrocytes

Astrocytes were seeded as previously described in 96-well plates. Cells were infected with FMT-eGFP or FMT-(MRB-G)-eGFP at MOI 10, 50, or 100. Cells were

imaged in real time using the IncuCyte live cell imaging system (Sartorius). Four images per well were taken every two hours for a total of 90 hours with the phase contrast and GFP channels. Representative images and total green object area per well values were analyzed using IncuCyte ZOOM software (Sartorius). Prism 8 software (GraphPad) was used to plot the mean and standard deviation of GFP area over time.

Live cell imaging

U343 or NHA cells were seeded into 35 mm glass-bottom dishes (Ibidi) at 1.2E5 and 6E4 cells/dish, respectively. For NHA seeding, dishes were pre-treated with collagen as previously described. After cells had grown to about 70% confluency, cells were bound with DiD-labeled FMT-(MRB-G) at MOI 100 for 1 hour at 4ºC, then washed with cold PBS three times. The sample was mounted on the 40X oil objective of a wide-field, epifluorescent DeltaVision Elite microscope (GE Life Sciences) with an environmental chamber maintained at 37ºC and 5% CO_2. The sample was quickly focused, and three regions containing cells bound by virus were selected. The dish was then flooded with 1.5 mL of warm phenol-free complete Astrocyte Media (ScienCell), or phenol-free DMEM (Gibco) supplemented with 5% FBS. A 9 µm z-stack with 3 x 3 µm slices was taken in the Cy5 and differential interference contrast (DIC) channels every 20 seconds for 1 hour. Time-lapse videos were deconvolved using softWoRx software (GE LifeSciences).

For experiments involving co-localization of DiD-labeled virions with endosomal markers, cells were transduced with Cell Light vectors (Thermo Fisher) expressing GFP fused with early endosome associated protein 1 (EEA1), late endosomal protein Rab7, or lysosomal-associated membrane protein 1 (LAMP1) at MOI 30, and incubated at

37ºC for 18 hours. Cells were infected with DiD-labeled virions and analyzed by live cell imaging as previously described in the FITC, Cy5, and DIC channels.

2.12 Image analysis

Imaris

Video files were analyzed using Imaris software (Oxford Instruments). Three regions of interest containing approximately 200 DiD-labeled virions were selected from each sample for analysis. The Imaris "Spots" function was used to track intensity traces of individual DiD-labeled virions over time. Virions with an estimated particle size between 0.2 and 1 μm^2 were included in the analysis, as previously described** [91,92]. The Brownian motion 3D tracking algorithm was used to predict the position of moving particles. Tracks of individual particles were ended when particles moved a distance greater than 3 μm, or a particle disappeared for longer than 40 seconds. Predicted particle tracks were adjusted manually for accuracy.

Identification of dequenching events using R

Identification of "dequenching" events from the track intensity traces was conducted in R (R Core Team, 2019). The R script was kindly written by Phil Charron at the CHEO Research Institute II, Ottawa, Canada. To eliminate outlier particles with abnormal intensity values, intensity traces with baseline intensity values falling between the 5^{th} and 95^{th} percentiles were chosen. Traces were then fit to a sigmoid curve with the following equation:

$$Y = a(1 + \exp^{(-b*(z-c))})$$

where initial values were set to a = 1, b = 1, and c = 1. Using the nlsLm formula from the minpack.lm package in R, optimized parameter values were then interpolated to

achieve a curve that fit the data efficiently. X values represented timepoints, and Y represented particle intensity values. An R^2 value was obtained using the following equation:

$$y = \Sigma_i(y_i - \hat{y})^2/\Sigma_i(y_i - \bar{y})^2$$

where y_i = particle intensity values, $\hat{y}_i$ = predicted intensity values, and $\bar{y}$ = mean particle intensity value. Intensity traces with a minimum R^2 value of 0.8 and a minimum 2-fold increase in particle intensity were identified as dequenching events. Prism 8 software (GraphPad) was used to plot the mean and standard deviation of the percentage of imaged particles that underwent dequenching. Prism was used to perform a one-way ANOVA, comparing percentage of dequenching amongst the different samples. ** = very significant, * = significant.

Colocalization of DiD-labeled particles with endosomal markers

Three regions of interest containing approximately 50 dequenching virions were selected from each sample, and the number of dequenching events was defined using the previously described R script. The Imaris “Spots” function was used to track DiD-labeled virions and labeled endosomes with a spot size of 0.8 μm. The Imaris “Colocalize Spots” function was used to colocalize endosome spots with virion spots over time. Colocalized spots were defined as spots with a maximum distance of 0.4 um between each other. Virions that dequenched in endosomes were defined as virions with overlapping periods of colocalization and dequenching. “% Dequenching” represented the number of virions dequenching when colocalized with labeled endosomes divided by the number of virions dequenching when not colocalized with labeled endosomes.

3. RESULTS

3.1 FMT infection in primary culture mouse neurons

Our lab had demonstrated that FMT is neurosafe when intracranially injected into mice. Interestingly, our preliminary data also demonstrated that intracranial injection of the FMT-(MRB-G) virus was neurotoxic, whereas the MRB-(FMT-G) virus was neurosafe (**Figure 1A**). These results suggested that the FMT glycoprotein may play a role in FMT's neurosafety. However, the role of the glycoprotein and other potential biological mechanisms underlying FMT's neurosafety have not been elucidated. Several studies have demonstrated that viral neuroattenuation is important for viral neurosafety [76,93–95]. This could suggest that FMT's neurosafety may partially depend on an attenuated capacity to infect normal brain cells. As well, FMT-(MRB-G)'s neurotoxicity may also correlate with a greater capacity to infect brain cells. Therefore, the infectivity of FMT and FMT-(MRB-G) in brain cells was explored *in vitro.*

Neurons from the cortex, striatum, and hippocampus as well as endothelial cells from the blood brain barrier (BBB) of CD-1 mice were cultured *in vitro* for this experiment. Cells were then infected with viruses encoding the enhanced green fluorescent protein (eGFP) (**Figure 1B**), where eGFP expression and fluorescence acted as a positive marker for infection [96–99]. Cells were infected with FMT and FMT-(MRB-G) expressing eGFP, known as FMT-eGFP and FMT-(MRB-G)-eGFP. As positive controls for neuronal infection, cells were also infected with VSV wildtype and VSVΔ51 encoding eGFP (labeled as VSV-eGFP and VSVΔ51-eGFP, respectively). MRB wildtype expressing eGFP (MRB-eGFP) was used as a potential positive control as well, since MRB is known to be neurovirulent [60]. eGFP fluorescence in infected neurons and BBB endothelial cells

was then monitored in real time using IncuCyte live cell imaging over the course of infection (**Figure 1C-F**).

At 20 hours post-infection, the GFP area of neurons and BBB endothelial cells infected with the positive control viruses VSV-eGFP and MRB-eGFP was very significant compared to the uninfected sample, confirming the neurovirulence of these viruses. VSVΔ51-eGFP infected neurons at similar levels to VSV-eGFP and MRB-eGFP as well. However, its infection within BBB endothelial cells was attenuated. This could be due to the higher expression and production of type 1 IFNs within BBB endothelial cells compared to neurons [87,100].

In contrast, the GFP area of all cells infected with FMT-eGFP was not significant compared to uninfected cells (**Figure 1E-F**). This suggested that FMT's capacity to infect neurons and endothelial cells of the BBB was attenuated. FMT-(MRB-G)-eGFP infection within the four brain cell populations was very significant, suggesting that this virus was neurovirulent. The contrast in neurovirulence between FMT-(MRB-G)-eGFP and FMT-eGFP implied that the FMT glycoprotein may play a role in FMT's neuroattenuation. Overall, these results demonstrated that FMT has an attenuated capacity to infect neurons relative to neurovirulent rhabdoviruses, and that this attenuation may be partially dependent on the FMT glycoprotein. This data also correlated neurovirulence observed *in vitro* with neurotoxicity seen *in vivo,* suggesting that FMT's neurosafety may depend on its attenuated capacity to infect brain cells.

Figure 2. FMT infection in primary culture mouse neurons is attenuated. (A) Survival of BALB/c mice after intracranial injection of FMT-(MRB-G) or MRB-(FMT-G) at 1E8 pfu. Experiment was kindly performed by Beta Yadollahi at the CHEO Research Institute II, Ottawa, Canada. N=5 biological replicates. (B) Schematic display of eGFP-expressing FMT, VSV, and MRB variants; viral genes are shown in grey, blue, and yellow, respectively. The red "M" gene in VSVΔ51-eGFP indicates a mutation in the M protein. (C) Primary culture mouse neurons of cortical, hippocampal, and striatal origin and endothelial cells from the blood brain barrier (BBB endothelial) were infected with the eGFP-expressing viruses illustrated in (B) at MOI 1 and 0.1. eGFP levels from infected cells were monitored in real time using IncuCyte live cell imaging. N=3 technical replicates. (D) A panel of representative images show phase contrast and GFP fluorescence microscopy images 20h post-infection in the four cell types. (E) eGFP levels of infected cells at 20 hours post-infection in the four cell types. Statistics: one-way ANOVA ($F(5,10) = 105.1$, $p < 0.0001$). Dunnett's post hoc test for multiple comparisons: ns = non-significant (FMT-eGFP versus Uninfected). Ns = non-significant. (F) A panel of representative images show overlay of phase contrast and GFP fluorescence microscopy images of blood brain barrier endothelial cells infected at MOI 0.01 over the course of 48h. Data in all figures represents group means +/- SD.

A

Virus	IC injection	Survival
FMT-(MRB-G)	1E8 pfu	0/5
MRB-(FMT-G)	1E8 pfu	5/5

B

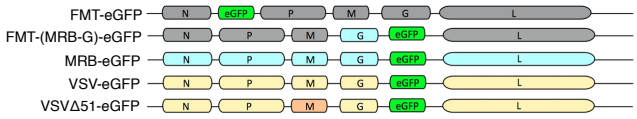

C

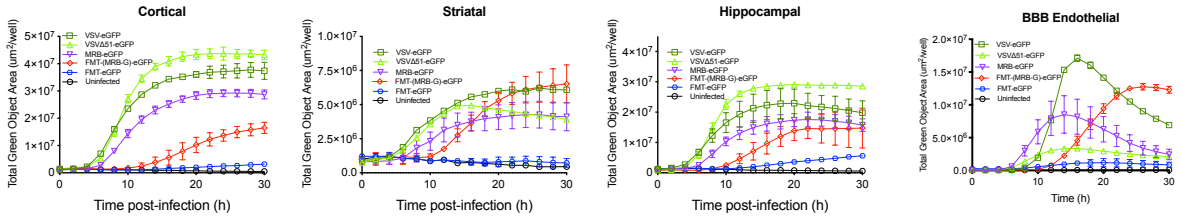

D

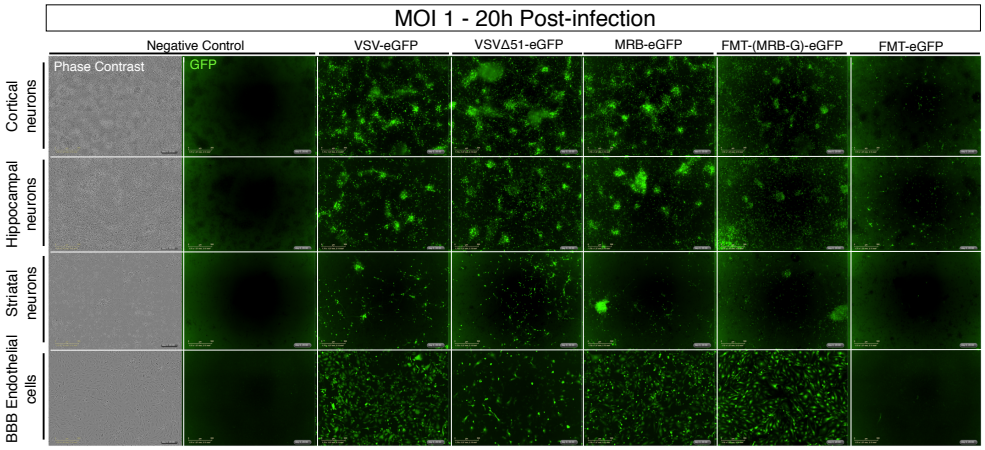

E

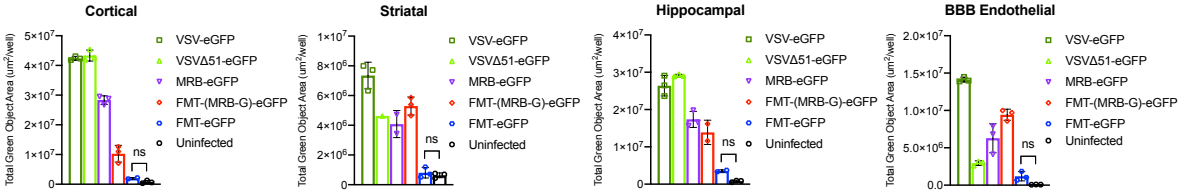

F

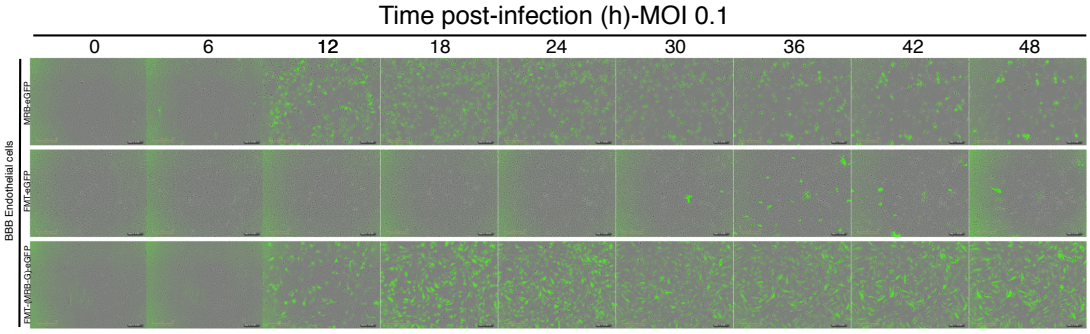

3.2 Comparing viral transcript abundance in normal human astrocytes infected with FMT-eGFP or FMT-(MRB-G)-eGFP

The contrast between FMT-eGFP and FMT-(MRB-G)-eGFP's neurovirulence profiles indicated that the FMT glycoprotein played a role in attenuating FMT infection in brain cells. Viral entry is a glycoprotein-dependent step in the viral replication cycle [31]. Therefore, we predicted that FMT viral entry was restricted relative to FMT-(MRB-G) entry. Since viral transcription is the first step to occur after entry in the rhabdoviral replication cycle [101], we assumed that FMT transcript levels would be attenuated if its viral entry was blocked. Thus, viral transcript abundance of FMT-eGFP and FMT-(MRB-G)-eGFP was analyzed in normal brain cells. With the aim of investigating FMT infection in human brain cells as well, this experiment was carried out in normal human astrocytes (NHA). To first determine the infectivity of FMT-eGFP or FMT-(MRB-G)-eGFP in human astrocytes, NHA cells were infected with both viruses and eGFP levels were monitored via IncuCyte live cell imaging (**Figure 2A, C**). To investigate viral transcript levels in these cells, the relative abundance of FMT nucleoprotein transcripts (FMT N) compared to cellular *Gapdh* transcripts was quantitatively analyzed in NHA cells infected with FMT-eGFP or FMT-(MRB-G)-eGFP at 0, 1, 2, 4, 8, 16, and 24 h post-infection (**Figure 2B**).

eGFP levels in FMT-eGFP and FMT-(MRB-G)-eGFP-infected cells were detected around 6 and 10 hours post-infection, respectively. This disparity in the timing of eGFP fluorescence was likely because eGFP was located after the nucleoprotein gene in FMT-eGFP and after the glycoprotein gene in FMT-(MRB-G)-eGFP. As rhabdoviral transcript abundance decreases with distance from the 3' promoter [102], the eGFP transgene in FMT-

eGFP-infected cells was likely expressed earlier and in more abundance than in FMT-(MRB-G)-eGFP-infected cells. In FMT-eGFP-infected cells, eGFP levels reached a plateau around 16 hours, and reached non-significant levels compared to uninfected cells at 24 hours. In contrast to FMT-eGFP, eGFP levels in FMT-(MRB-G)-eGFP-infected cells continued to increase past 16 hours, and reached significant levels compared to uninfected cells at 24 hours. These results indicated that FMT infection was blocked in human astrocytes as well, and that the glycoprotein-dependent differential between FMT-eGFP and FMT-(MRB-G)-eGFP may also exist within astrocytes.

Similar to the eGFP abundance, FMT N transcript abundance began to increase around 8 hours post-infection with FMT-eGFP or FMT-(MRB-G)-eGFP. However, by 16 hours post-infection, transcript abundance in FMT-eGFP-infected cells had stopped increasing, and reached non-significant levels compared to uninfected cells at 24 hours. This correlated well with FMT-eGFP's eGFP expression kinetics. In contrast, FMT-(MRB-G)-eGFP transcript levels continued to increase up to 24 hours post-infection, where its levels were very significant relative to uninfected cells. Therefore, FMT-eGFP's transcript abundance was attenuated relative to FMT-(MRB-G)-eGFP in astrocytes. This could suggest that the glycoprotein-dependent block to FMT infection may occur prior to viral transcription. Therefore, it is feasible that FMT infection is blocked at the level of viral entry.

Figure 2. FMT-eGFP and FMT-(MRB-G)-eGFP infection in normal human astrocytes. (A) NHA cells were infected with FMT-eGFP or FMT-(MRB-G)-eGFP at MOI 5. eGFP levels in infected cells were monitored in real time using IncuCyte live cell imaging. Statistics: two-way ANOVA ($F(24, 72) = 59.86$, $p < 0.0001$). Tukey's post hoc test for multiple comparisons: * = significant, ns = non-significant (FMT-(MRB-G)-eGFP or FMT-eGFP versus Uninfected at 24 hours post-infection, respectively). N=3 technical replicates. (B) Relative abundance of FMT N transcripts compared to human *Gapdh* transcripts in infected NHA cells. FMT N transcripts and human *Gapdh* transcripts were quantitatively analyzed at 0, 1, 2, 4, 8, 16, and 24 h post-infection via qPCR. Statistics: two-way ANOVA ($F(12, 42) = 86.65$, $p < 0.0001$). Tukey's post hoc test for multiple comparisons: *** = very significant, * = significant, ns = non-significant (FMT-(MRB-G)-eGFP or FMT-eGFP versus Uninfected at 24 hours post-infection, respectively). N = 3 technical replicates. (C) A panel of representative images show phase contrast and GFP fluorescence microscopy images of the infected NHA cells from the experiments in panels (A) and (B) over the course of infection. Data in all figures represents group means +/- SD.

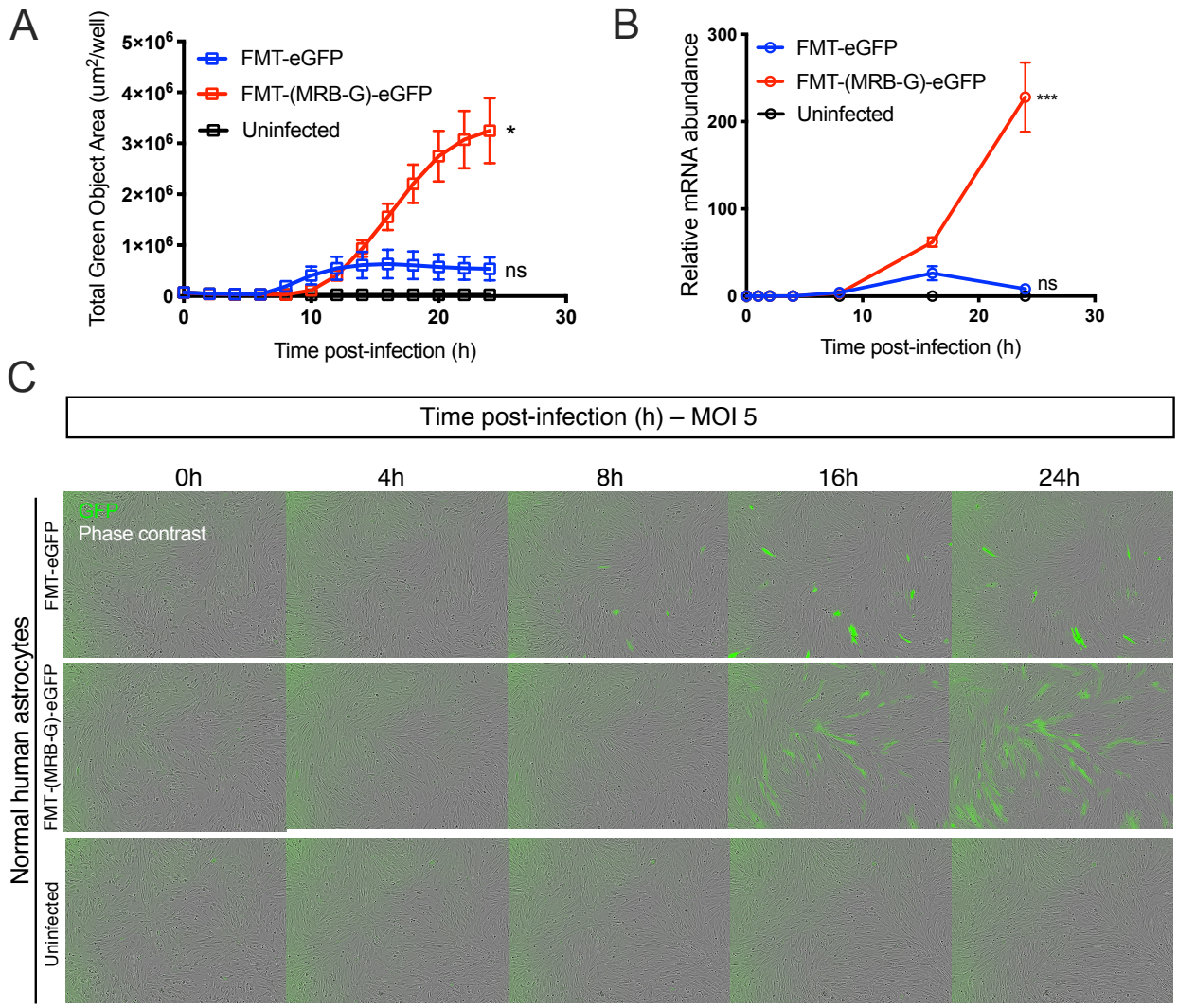
A
Total Green Object Area (um²/well)
5×10⁶
4×10⁶
3×10⁶
2×10⁶
1×10⁶
0
FMT-eGFP
FMT-(MRB-G)-eGFP
Uninfected
*
ns
0
10
20
30
Time post-infection (h)
B
Relative mRNA abundance
300
200
100
0
FMT-eGFP
FMT-(MRB-G)-eGFP
Uninfected
***
ns
0
10
20
30
Time post-infection (h)
C
Time post-infection (h) – MOI 5
0h
4h
8h
16h
24h
Normal human astrocytes
FMT-eGFP
FMT-(MRB-G)-eGFP
Uninfected
GFP
Phase contrast

3.3 Investigating the type 1 interferon response in FMT-infected brain cells

Our lab had previously demonstrated that FMT infection in human and mouse fibroblasts induces interferon beta 1 expression which restricts its infection in these cells. It is therefore possible that FMT infection in astrocytes and neurons is restricted by interferon beta as well. Astrocytes act as a primary producer of interferon beta within the brain [87]. Thus, interferon beta 1 mRNA and protein production were measured in astrocytes infected with FMT, and the sensitivity of FMT's replication cycle to interferon beta signaling was measured in cortical neurons. As well, the differential between FMT-eGFP and FMT-(MRB-G)-eGFP infection in brain cells could be explained by a differential in the induction of interferon beta expression. Thus, interferon beta expression was examined in astrocytes infected with FMT-(MRB-G)-eGFP as well.

To explore the induction of interferon beta in astrocytes infected with FMT-eGFP or FMT-(MRB-G)-eGFP, the abundance of *Ifnb1* mRNA in NHA cells infected with either virus was quantitatively analyzed by qPCR at 0, 1, 2, 4, 8, 16, and 24 hours post-infection (**Figure 3A**). Both viruses induced very significant *Ifnb1* expression in astrocytes. However, FMT-eGFP appeared to induce *Ifnb1* expression 8 hours earlier than FMT-(MRB-G)-eGFP (**Figure 3B**). At 16 hours post-infection, *Ifnb1* expression in FMT-eGFP-infected astrocytes was very significant relative to uninfected cells. However, *Ifnb1* expression in FMT-(MRB-G)-eGFP-infected astrocytes did not reach significant levels until 24 hours post-infection. This suggests that the glycoprotein may affect when the type 1 interferon response is induced. Therefore, the early induction of the type 1 interferon response in FMT-eGFP-infected astrocytes could have inhibited

FMT infection, whereas FMT-(MRB-G)-eGFP's delayed interferon induction may have failed to inhibit its infection before viral spreading occurred.

Next, we sought to determine if the expression of *Ifnb1* would be correlated with interferon beta 1 protein (IFNβ1) expression in FMT-eGFP or FMT-(MRB-G)-eGFP-infected astrocytes as well. To test this, NHA cells were infected with FMT-eGFP, FMT-(MRB-G)-eGFP, or MRB-eGFP. MRB-eGFP acted as a negative control for IFNβ1 protein induction, as the wildtype Maraba matrix protein inhibits *Ifnb1* expression [60]. At 24 hours post-infection, IFNβ1 protein concentration was measured in the supernatant of infected cells via an enzyme-linked immunosorbent assay (ELISA) (**Figure 3B**). As expected, IFNβ1 concentration from the supernatant of MRB-eGFP-infected astrocytes was non-significant relative to the uninfected control, with a mean concentration of about 8 pg/ml. In contrast, the supernatant IFNβ1 concentration from both FMT-eGFP- and FMT-(MRB-G)-eGFP-infected astrocytes was very significant relative to the uninfected control sample, with a mean concentration of about 216 and 214 pg/ml, respectively. However, it is important to note that the ELISA kit was saturated for both the FMT-eGFP and FMT-(MRB-G)-eGFP samples; therefore, the specific concentration is likely not accurate. Despite this, this result suggested that both viruses are capable of inducing significant IFNβ1 expression, which correlated well with the *Ifnb1* expression data. As well, FMT's significant expression of IFNβ1 protein may have restricted this virus' infection within astrocytes.

Since we had confirmed that FMT induced IFNβ1 expression, the sensitivity of FMT's replication cycle to IFNβ1 signaling was examined as well. In this experiment, mouse cortical neurons were infected with FMT-eGFP at an MOI of 0.1, then incubated

with interferon beta 1 (IFNβ1) neutralizing antibodies or control immunoglobulin (IgG) antibodies. Neurons were also infected with MRB-eGFP as a control; as this virus can inhibit IFNβ1, its replication cycle should not be inhibited by IFNβ1-neutralizing antibodies. To measure differences in the levels of infection for these viruses, eGFP fluorescence of the infected cells was monitored via IncuCyte live cell imaging (**Figure 3C-D**).

As expected, eGFP levels in MRB-eGFP-infected cells were not significantly impacted by IFNβ1 neutralization at 24 hours post-infection, confirming this virus as a negative control for this assay. (**Figure 3E**). In contrast, eGFP levels in FMT-eGFP-infected neurons at 24 hours were very significant in the presence of IFNβ1-neutralizing antibodies compared to eGFP levels with control antibodies. This suggested that FMT induced IFNβ1 production within cortical neurons. As well, the increase in FMT infection upon blocking IFNβ1 suggested that IFNβ1-dependent signaling restricted FMT infection within neurons.

Figure 3. Characterization of the type 1 interferon response in FMT infection of astrocytes and cortical neurons. (A) Abundance of *Ifnb1* transcripts relative to host *Gapdh* transcripts in normal human astrocytes (NHA) infected with FMT-eGFP or FMT(MRB-G)-eGFP at MOI 5. *Ifnb1* and *Gapdh* transcripts were quantitatively analyzed at 0, 1, 2, 4, 8, 16, and 24 h post-infection via qPCR. Statistics: two-way ANOVA ($F(12, 42) = 55.23$, $p < 0.0001$). Tukey's post hoc test for multiple comparisons: *** = very significant, ### = very significant, ns = non-significant (FMT-eGFP or FMT-(MRB-G)-eGFP versus Uninfected at 16 and 24 hours post-infection). (B) Concentration of IFNβ1 protein from the supernatant of NHA cells infected with FMT-eGFP, FMT-(MRB-G)-eGFP, or MRB-eGFP at MOI 5. Supernatant of infected cells was collected 24 hours post-infection. IFNβ1 protein concentration was quantified via ELISA analysis. Statistics: one-way ANOVA ($F(3, 4) = 6941$, $p < 0.0001$). Tukey's post hoc test for multiple comparisons: *** = very significant, ### = very significant, ns = non-significant (FMT-eGFP, FMT-(MRB-G)-eGFP, or MRB-eGFP versus Uninfected). N = 2 technical replicates. (C) Total eGFP levels of cortical neurons infected with MRB-eGFP or FMT-eGFP in the presence or absence of IFNβ1-blocking antibodies (α-IFNβ1) or control IgG antibodies. Neurons were infected at MOI 0.1, then incubated with antibodies. Total eGFP fluorescence from infected cells was monitored in real time using IncuCyte live cell imaging. (D) A panel of representative images show phase contrast and GFP fluorescence microscopy images of the infected cortical neurons treated with IFNβ1-blocking antibodies at 24h post-infection. (E) Total eGFP area at 24 hours post-infection from experiment in panel (C). Statistics: unpaired t test; $t(6.508) = 4$, $p = 0.0029$) for FMT-eGFP with 10X α-IFNβ1 versus 10X IgG. Unpaired t test; $t(1.177) = 4$, $p = 0.3045$) for MRB-eGFP with 10X α-IFNβ1 versus 10X IgG. ** = very significant, ns = not significant. N = 3 technical replicates. Data in all figures represents group means +/- SD.

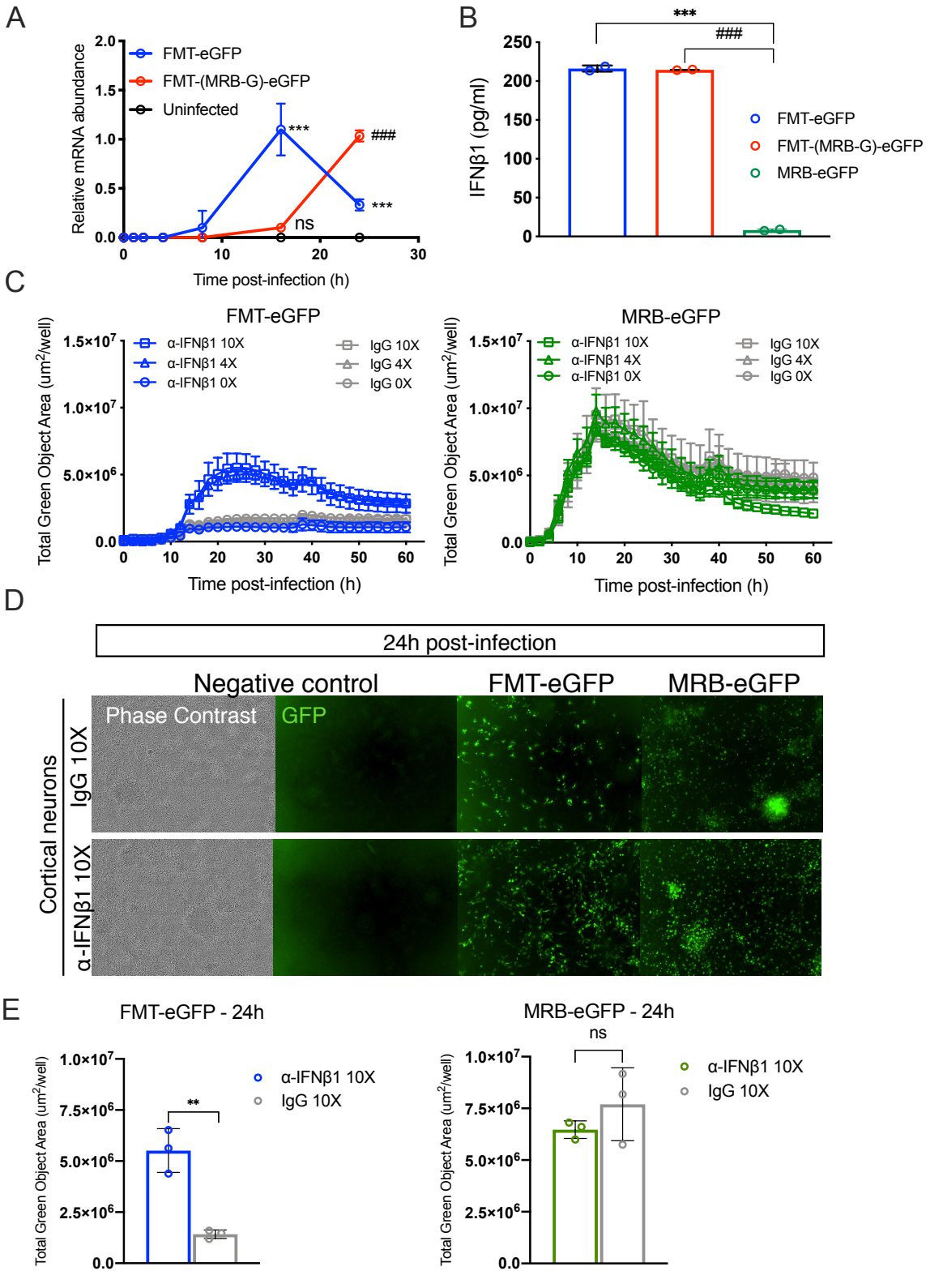
A
Relative mRNA abundance
FMT-eGFP
FMT-(MRB-G)-eGFP
Uninfected
***
###
***
ns
Time post-infection (h)
B
IFNβ1 (pg/ml)
***
###
FMT-eGFP
FMT-(MRB-G)-eGFP
MRB-eGFP
C
FMT-eGFP
MRB-eGFP
Total Green Object Area (um²/well)
α-IFNβ1 10X
α-IFNβ1 4X
α-IFNβ1 0X
IgG 10X
IgG 4X
IgG 0X
Time post-infection (h)
D
24h post-infection
Negative control
FMT-eGFP
MRB-eGFP
Phase Contrast
GFP
Cortical neurons
IgG 10X
α-IFNβ1 10X
E
FMT-eGFP - 24h
MRB-eGFP - 24h
Total Green Object Area (um²/well)
**
ns
α-IFNβ1 10X
IgG 10X

3.4 Comparing viral transcript abundance in glioblastoma cells infected with FMT-eGFP and FMT-(MRB-G)-eGFP

Our viral transcription experiment suggested that viral entry mediated by the FMT glycoprotein may be attenuated relative to the MRB glycoprotein in astrocytes. However, FMT and MRB are both highly infectious in brain tumour cells [60]. This could suggest that FMT viral entry is more efficient within brain cancer cells compared astrocytes. As well, viral entry mediated by the FMT and MRB glycoproteins may be very similar within brain tumour cells. To test this, we evaluated the viral transcription kinetics and eGFP expression kinetics of FMT-eGFP and FMT-(MRB-G)-eGFP in U343 cells, a human glioblastoma cell line that is known to be well infected by FMT [60]. In this experiment, U343 cells were infected with FMT-eGFP and FMT-(MRB-G)-eGFP at MOI 5. The relative mRNA abundance of FMT N mRNA compared to *Gapdh* mRNA was determined by qPCR over the course of 24 hours (**Figure 4A**). To compare infection levels of the two viruses, eGFP levels of infected cells were monitored using IncuCyte live cell imaging (**Figure 4B-C**).

As expected, eGFP expression revealed that FMT-eGFP was very infectious within U343 cells, confirming FMT's tropism for brain cancer cells. The previously suggested glycoprotein-dependent nature of FMT's selectivity could indicate that FMT entry is more efficient within brain cancer cells relative to normal brain cells. Interestingly, eGFP levels in FMT-eGFP-and FMT-(MRB-G)-eGFP-infected U343 cells were very similar to each other over the course of infection (**Figure 4A, C**). Viral transcript levels were very similar between the two viruses as well (**Figure 4B**). The comparable eGFP expression and

transcription kinetics of FMT-eGFP and FMT-(MRB-G)-eGFP in U343 cells could suggest that these two viruses enter U343 cells at similar efficiencies.

Figure 4. FMT-eGFP and FMT-(MRB-G)-eGFP infection in U343 cells. (A) Human U343 glioblastoma cells were infected with FMT-eGFP or FMT-(MRB-G)-eGFP at MOI 5. Total GFP fluorescence from infected cells was monitored in real time using IncuCyte live cell imaging. N = 3 technical replicates. (B) Relative abundance of FMT N transcripts compared to human *Gapdh* transcripts in cell infected with FMT-eGFP or FMT-(MRB-G)-eGFP at MOI 5. FMT N transcripts and human *Gapdh* transcripts were quantitatively analyzed at 0, 1, 2, 4, 8, 16, and 24 h post-infection. N = 3 technical replicates. (C) A panel of representative images show phase contrast and GFP fluorescence microscopy images of the infected U343 cells from the experiment in panels (A) and (B) over the course of 24 h post-infection. Data in all figures represents group means +/- SD.

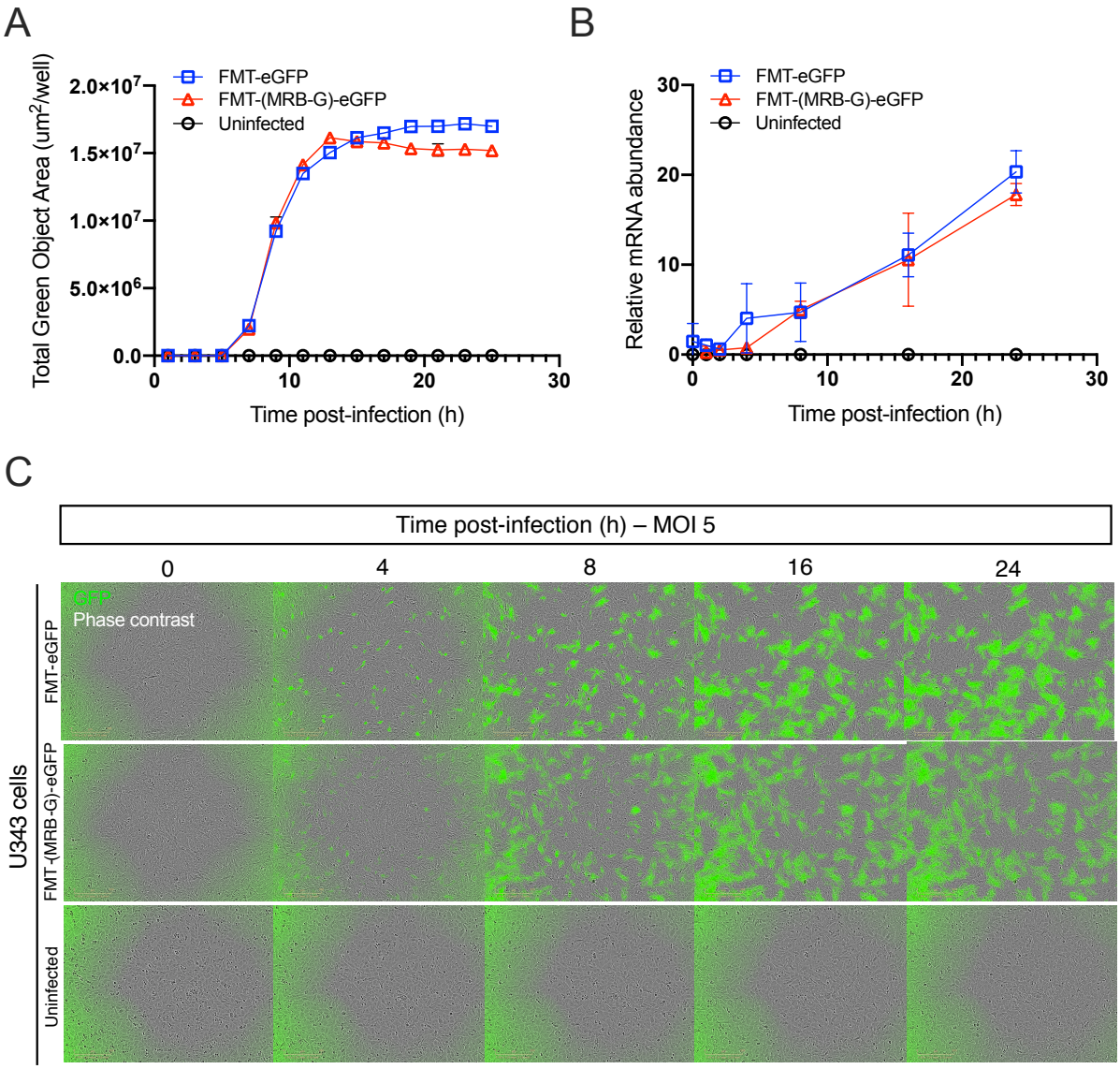
A
Total Green Object Area (um²/well)
2.0×10⁷
1.5×10⁷
1.0×10⁷
5.0×10⁶
0.0
0
10
20
30
Time post-infection (h)
FMT-eGFP
FMT-(MRB-G)-eGFP
Uninfected
B
Relative mRNA abundance
30
20
10
0
0
10
20
30
Time post-infection (h)
FMT-eGFP
FMT-(MRB-G)-eGFP
Uninfected
C
Time post-infection (h) – MOI 5
0
4
8
16
24
U343 cells
FMT-eGFP
FMT-(MRB-G)-eGFP
Uninfected
GFP
Phase contrast

3.5 Viral attachment of FMT-eGFP and FMT-(MRB-G)-eGFP in U343 and NHA cells

FMT-eGFP's attenuated viral transcript abundance in astrocytes implied that FMT's replication cycle was blocked at a step prior to viral transcription. As well, the contrast in transcript abundance between FMT-eGFP and FMT-(MRB-G)-eGFP-infected cells suggested that the inhibition of FMT infection was glycoprotein-dependent. Since viral entry is a glycoprotein-dependent step that precedes viral transcription [103–105], FMT's replication cycle could be blocked at the level of viral entry in astrocytes. As viral attachment to the cell surface is the first step of viral entry [106], it is possible that FMT-eGFP's lower infectivity in astrocytes could be due to lower levels of viral attachment relative to FMT-(MRB-G)-eGFP. Therefore, we compared the viral attachment levels of FMT-eGFP to FMT-(MRB-G)-eGFP in astrocytes. Viral attachment was also studied in U343 cells. As the infection kinetics of FMT-eGFP and FMT-(MRB-G)-eGFP were very similar in U343 cells, we predicted that these two viruses would also share similar levels of viral attachment. To test this, NHA and U343 cells were infected with the two viruses at 4°C for 1 hour to allow attachment without internalization. The quantity of FMT-eGFP or FMT-(MRB-G)-eGFP viral genomes relative to cellular *Gapdh* mRNA was measured via qPCR (**Figure 5A**). The relative quantity of bound FMT-eGFP or FMT-(MRB-G)-eGFP virions was also observed via confocal microscopy (**Figure 5B**).

To confirm that differences in viral attachment levels between FMT-eGFP and FMT-(MRB-G)-eGFP were not due to differences in the amount of virus added, we first confirmed the titre of each virus via plaque assay and qPCR (**Figure 5C**). Our titre determined via plaque assay was very similar to the titre determined by qPCR for both

viruses. Therefore, we were confident in the titre used within this experiment and could therefore trust quantitative differences in the viral attachment of these two viruses.

Interestingly, viral attachment of FMT-eGFP virions was approximately 2.4-fold lower than FMT-(MRB-G)-eGFP in astrocytes. This correlated with the results from the confocal images, where less FMT-eGFP virions were observed binding to astrocytes compared to FMT-(MRB-G)-eGFP. Together, these results suggested that FMT-eGFP's viral attachment to astrocytes may be limited relative to FMT-(MRB-G)-eGFP, which could explain FMT's attenuated infection in these cells. Despite having similar infection kinetics in brain cancer cells, FMT-eGFP and FMT-(MRB-G)-eGFP demonstrated significantly different levels of viral attachment to U343 cells as well. Viral attachment of FMT-eGFP was 3.3-fold lower than FMT-(MRB-G)-eGFP in U343 cells. As well, less FMT-eGFP particles were observed binding to U343 cells compared to FMT-(MRB-G)-eGFP by confocal microscopy. However, the degree of FMT-eGFP's viral attachment to U343 cells may have reached a minimum threshold for infection that was not achieved in astrocytes. Overall, attenuated viral attachment may be a contributing factor in FMT's lack of tropism for astrocytes.

Figure 5. Viral attachment of FMT-eGFP and FMT-(MRB-G)-eGFP in U343 and NHA cells. (A) Quantitation of FMT-eGFP or FMT-(MRB-G)-eGFP bound to U343 or NHA cells. FMT-eGFP or FMT-(MRB-G)-eGFP virus were bound to U343 or NHA cells at MOI 10 for 1 hour at 4°C. The relative RNA abundance of viral genomes to cellular *Gapdh* mRNA was determined by qPCR analysis. Statistics: unpaired t test; t(7.519) = 4, p = 0.0017) for FMT-eGFP versus FMT-(MRB-G)-eGFP in U343 cells. Unpaired t test; t(4.544) = 4, p = 0.0105) for FMT-eGFP versus FMT-(MRB-G)-eGFP in NHA cells. ** = very significant, # = significant. N = 3 technical replicates. (B) U343 or NHA cells were bound with FMT-eGFP or FMT-(MRB-G)-eGFP at MOI 50 for 1 hour at 4°C. Cells were fixed and stained with anti-FMT antibody and DAPI, then bound virus was visualized by confocal microscopy. Image brightness was adjusted equally amongst all images using ImageJ software. N = 3 technical replicates. (C) Confirmation of viral titres. Viral stocks used in experiments (A) and (B) were titred via plaque assay and qPCR. Viral RNA extraction for the qPCR experiment was kindly performed by Matteo Da Ros at the CHEO Research Institute II, Ottawa, Canada. qPCR of the viral titres was kindly performed by Phil Charron at the CHEO Research Institute II, Ottawa, Canada. Statistics: unpaired t test; t(1.152) = 4, p = 0.3134) comparing titre of FMT-eGFP via qPCR versus plaque assay. Unpaired t test; t(0.5516) = 4, p = 0.6106) comparing titre of FMT-(MRB-G)-eGFP via qPCR versus plaque assay. Ns = not significant. N = 3 biological replicates. Data in all figures represents group means +/- SD.

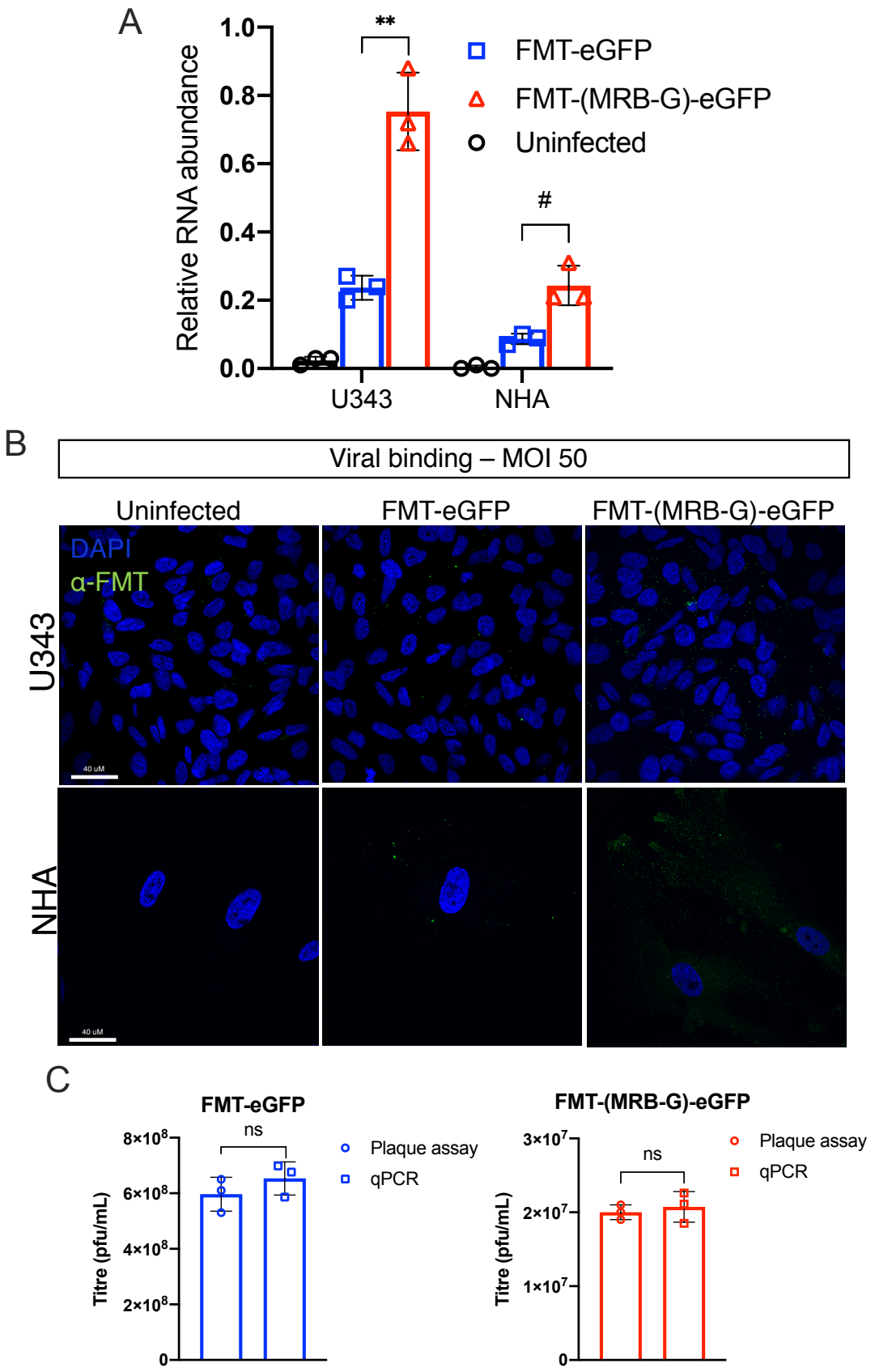
A
Relative RNA abundance
1.0
0.8
0.6
0.4
0.2
0.0
**
#
FMT-eGFP
FMT-(MRB-G)-eGFP
Uninfected
U343
NHA
B
Viral binding – MOI 50
Uninfected
FMT-eGFP
FMT-(MRB-G)-eGFP
DAPI
α-FMT
U343
NHA
40 uM
C
FMT-eGFP
FMT-(MRB-G)-eGFP
Titre (pfu/mL)
8×10^8
6×10^8
4×10^8
2×10^8
0
3×10^7
2×10^7
1×10^7
ns
Plaque assay
qPCR

3.6 FMT fusion in U343 cells

Our previous results suggested that FMT's viral attachment to astrocytes may be restricted, which could inhibit its infection in these cells. However, FMT's entry may also be inhibited at the level of viral fusion in astrocytes. Antiviral proteins or host degradation pathways can restrict viral fusion, thus inhibiting viral infection [107–109]. FMT-(MRB-G)-eGFP's fusion process could be more efficient and/or productive in astrocytes compared to FMT-eGFP as well. Additionally, FMT fusion may proceed more effectively in brain cancer cells relative to astrocytes. We therefore sought to study FMT and FMT-(MRB-G)'s viral fusion kinetics in astrocytes and U343 cells. In order to select the correct assay for studying viral fusion kinetics, we sought to determine how FMT and FMT-(MRB-G) viral fusion was triggered. Many rhabdoviruses such as VSV enter cells via endocytosis, and require the low pH of endosomes to trigger viral fusion [110–112]. We therefore predicted that FMT and FMT-(MRB-G) viral fusion would similarly require endosome acidification.

To investigate this hypothesis, the sensitivity of FMT and FMT-(MRB-G)'s viral fusion to endosome acidification was studied in U343 cells, as these cells are successfully infected by FMT. We determined the sensitivity of FMT viral fusion to endosome acidification by incubating U343 cells with drug inhibitors of this process. The weak bases ammonium chloride (NH4Cl) and chloroquine were used, as they accumulate in and raise the pH of endosomes [113,114]. We also used bafilomycin B1, a specific inhibitor of the vacuolar-ATPase enzyme which is responsible for endosome acidification [115]. After these drug inhibitors were added, cells were infected with FMT-eGFP, FMT-(MRB-G)-eGFP, MRB-eGFP, VSV-eGFP, or vaccinia virus expressing

eGFP (VACV-eGFP); cells were then imaged using IncuCyte live cell imaging (**Figure 6A, B, D**). As successful viral fusion results in viral gene expression, GFP fluorescence was used as a positive marker for viral fusion. Since VSV requires endosome acidification for its viral fusion, VSV-eGFP was used as a positive control. As MRB and VSV share similar infection kinetics [60], we expected MRB-eGFP and FMT-(MRB-G)-eGFP to be similarly sensitive to endosome acidification. Vaccinia virus can fuse directly with the plasma membrane or in endosomes, meaning its fusion process can be pH-independent or pH-dependent depending on the host cell [116,117]. Therefore, this virus was used a potential negative control as its entry in U343 cells could be pH-independent. To determine if eGFP expression was inhibited indirectly by drug-induced cytotoxicity, cell viability in the presence of the drug inhibitors was tested using red YOYO-3 staining. The RFP fluorescence was then quantified using IncuCyte live cell imaging (**Figure 6C**).

Through analyzing YOYO-3 staining, no significant changes in cell viability were observed with any of the drugs tested. Therefore, any differences in eGFP expression could be attributed to the sensitivity of viral fusion to endosome acidification. As expected, eGFP levels in cells infected with MRB-eGFP, VSV-eGFP, or FMT-(MRB-G)-eGFP were significantly inhibited with all three drug inhibitors in a dose-dependent manner. This demonstrated that the fusion of these viruses may be pH-dependent, suggesting that they may fuse in endosomes in U343 cells. eGFP levels in cells infected with FMT-eGFP or VACV-eGFP were also significantly inhibited by all three drugs, suggesting that their viral fusion within U343 cells may be triggered by low pH. Interestingly, FMT-eGFP and VACV-eGFP infection appeared to be less sensitive to

chloroquine-mediated inhibition compared to the other viruses. VACV-eGFP was less sensitive to NH4Cl and bafilomycin B1 inhibition as well. However, studies have demonstrated that viruses which fuse in lysosomes are often less sensitive to endosome acidification inhibitors [118]. This suggested that FMT and VACV may have fused in lysosomes. In conclusion, these results demonstrated that viral fusion of FMT may be triggered by low pH in lysosomes.

Figure 6. Effect of endosome acidification drug inhibitors on FMT viral fusion in U343 cells. U343 cells were incubated with increasing concentrations of bafilomycin B1, chloroquine, or ammonium chloride (NH4Cl) for 1 hour. Cells were then infected with FMT-eGFP, FMT-(MRB-G)-eGFP, MRB-eGFP, VSV-eGFP, or VACV-eGFP at MOI 0.1. (A) Total eGFP fluorescence from infected cells was monitored in real time using IncuCyte live cell imaging. (B) eGFP levels of infected cells at 14 hours post-infection. Statistics: one-way ANOVA ($F(3, 8) = 5521$, $p < 0.0001$, MRB-eGFP); ($F(3, 8) = 576.7$, $p < 0.0001$, FMT-(MRB-G)-eGFP); ($F(3, 8) = 178.5$, $p < 0.0001$, FMT-eGFP); ($F(3, 7) = 26051$, $p < 0.0001$, VSV-eGFP); ($F(3, 7) = 801.8$, $p < 0.0001$, VACV-eGFP). No Drug versus Bafilomycin B1, Chloroquine, or NH4Cl. Dunnett's post hoc test for multiple comparisons: * = significant, *** = very significant. (C) Cytotoxicity of the drug inhibitors. U343 cells were incubated with increasing concentrations of the three drugs in the presence of YOYO-3 and imaged in the phase and RFP channels using IncuCyte live cell imaging. Red object count represents the total number of YOYO-3 positive cells per well. (D) A panel of representative images show phase contrast and GFP fluorescence microscopy images of FMT-eGFP and FMT-(MRB-G)-eGFP infected U343 cells in the presence of bafilomycin B1 at 20 hours post-infection.

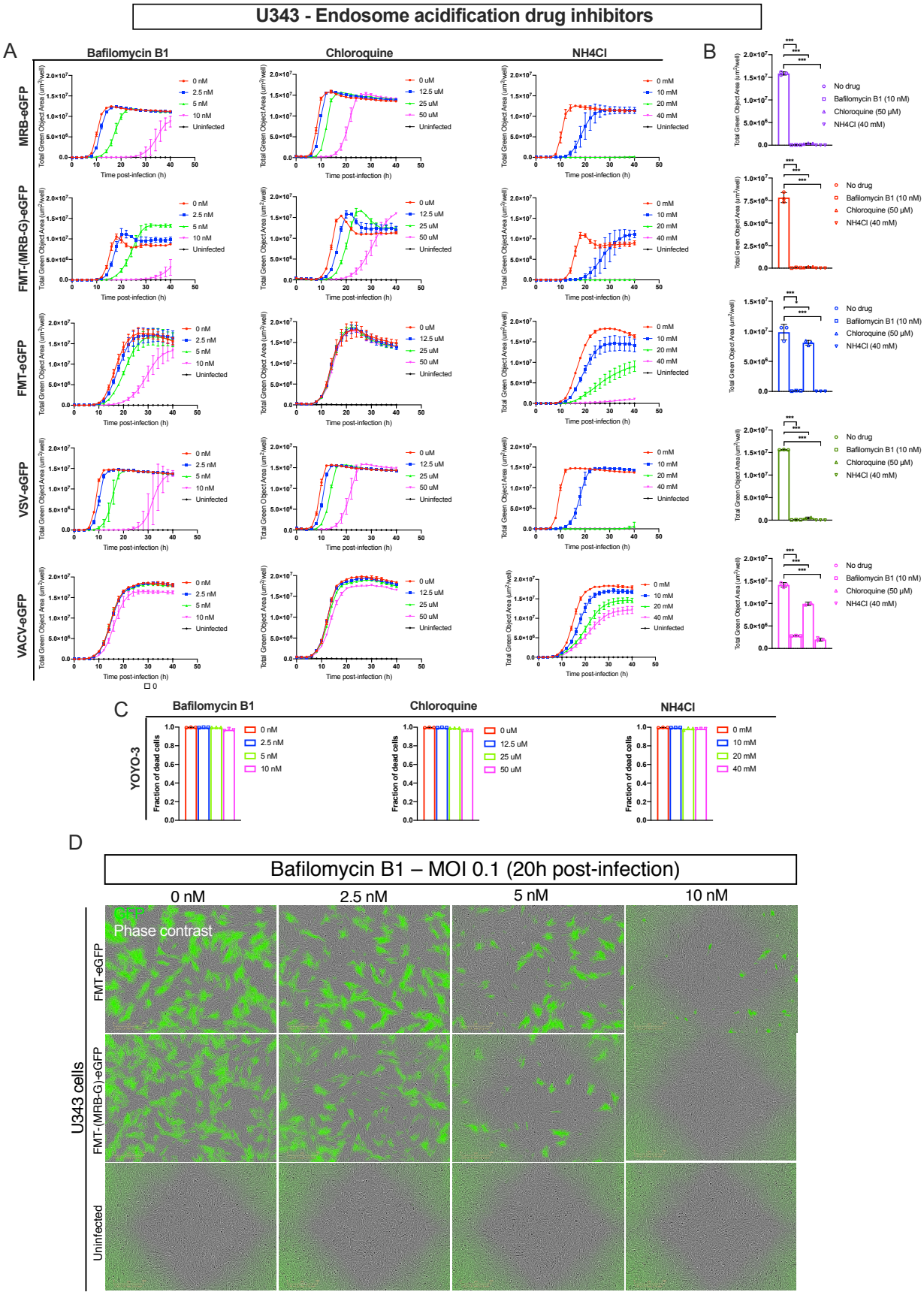
U343 - Endosome acidification drug inhibitors
A
Bafilomycin B1
Chloroquine
NH4Cl
MRB-eGFP
FMT-(MRB-G)-eGFP
FMT-eGFP
VSV-eGFP
VACV-eGFP
Total Green Object Area (um²/well)
Time post-infection (h)
0 nM
2.5 nM
5 nM
10 nM
Uninfected
0 uM
12.5 uM
25 uM
50 uM
0 mM
10 mM
20 mM
40 mM
B
No drug
Bafilomycin B1 (10 nM)
Chloroquine (50 μM)
NH4Cl (40 mM)
C
YOYO-3
Fraction of dead cells
D
Bafilomycin B1 – MOI 0.1 (20h post-infection)
0 nM
2.5 nM
5 nM
10 nM
Phase contrast
U343 cells
FMT-eGFP
FMT-(MRB-G)-eGFP
Uninfected

3.7 Characterization of DiD-labeled FMT and FMT-(MRB-G)

Our data suggested that FMT viral entry may be restricted in astrocytes, yet unhindered in U343 cells. Thus, it seemed reasonable to explore if FMT entry was inhibited at the level of viral fusion in astrocytes, but less restricted in U343 cells. As well, we predicted that viral fusion of FMT-(MRB-G) would be relatively unhindered in both cell lines.

To test this, viral fusion of FMT and FMT-(MRB-G) was quantified in NHA and U343 cells using a lipid mixing assay. In this assay, viruses were labeled with the lipophilic, self-quenching fluorescent dye 1,1′-dioctadecyl-3,3,3′,3′-tetramethylindodicarbocyanine (DiD). DiD remains self-quenched in the viral membrane until viral fusion occurs, where the dye dilutes into the host membrane. If a viral particle fuses in an endosome or lysosome, the dye dilutes and “dequenches”, resulting in an increase in DiD fluorescence intensity [119,120]. These increases in DiD intensity can be monitored by imaging cells infected with DiD-labeled viruses at high MOIs through time-lapse live cell microscopy.

First, FMT and FMT-(MRB-G) were indirectly labeled with DiD according to the protocol described by the Langlois laboratory at the University of Ottawa [121]. To indirectly label the viruses, vero cells were labeled with 25 μM DiD (or PBS as an unlabeled control), then infected with FMT, FMT-(MRB-G), or PBS (for the uninfected control). As rhabdoviruses are enveloped viruses [122], the DiD dye should be incorporated into the viral membrane which buds out from host cell membrane. After sufficient infection occurred, the supernatant containing the labeled viruses was collected, filtered, and titred by the plaque assay technique. Titres revealed that DiD-

labeled veros produced less virions than unlabeled veros (**Figure 7B**). Labeling likely reduced cell viability to an extent, which could have reduced its ability to produce virus. However, the titres of the DiD-labeled FMT and FMT-(MRB-G) (1.5E8 and 5.95E7 pfu/mL, respectively) were sufficiently high for use in the lipid mixing assay. These titres also indicated that the labeled particles were infectious and could therefore be used to study viral entry.

To validate labeling, the DiD fluorescence intensity of the labeled FMT, FMT-(MRB-G), and uninfected preparations was determined. Labeled supernatants were attached to U343 cells and imaged via confocal microscopy. DiD-labeled particles were observed clustering around nuclei (**Figure 7A**). Particles were approximately 0.1 to 1 um in length, as expected for discrete rhabdovirus particles [123]. Fluorescence intensities of labeled particles ranged from 30 to 1200 arbitrary units (au) (**Figure S1**), with an average intensity of approximately 370 au's, as previously observed [91,92,124]. As well, no labeled particles were observed in uninfected samples from labeled veros, suggesting that fluorescent particles from infected samples were indeed labeled viruses and not labeled cell matter. Therefore, these results suggested that viruses were successfully labeled with DiD.

In order to quantify large numbers of fusion events for analysis, lipid mixing assays are typically performed at high MOIs [91,92]. However, we first sought to determine if infecting astrocytes with FMT or FMT-(MRB-G) at high MOIs would change the infection levels within these cells. To test this, astrocytes were infected with FMT-eGFP or FMT-(MRB-B)-eGFP at MOI 0, 50, and 100. eGFP expression was used as a marker for positive infection (**Figure S2**). It appeared that FMT-eGFP

infection was similarly attenuated at all MOIs tested. As well, FMT-(MRB-G)-eGFP levels did not change drastically between the different MOIs. Therefore, this suggested that infection at high MOIs would not affect the biology of infection.

As previously defined [91,92,124], a true dequenching event has a minimum two-fold increase in DiD fluorescence intensity that occurs in a sigmoidal fashion. To determine if DiD within the viral membrane was capable of dequenching upon lipid mixing, the fluorescence intensity of DiD-labeled particles was monitored during infection. As a positive control for viral fusion, U343 cells were infected with DiD-labeled FMT-(MRB-G) at MOI 100. The DiD fluorescence intensity of the viral particles was then tracked using time-lapse live cell imaging. As expected, sharp increases in the DiD fluorescence intensity of DiD-labeled FMT-(MRB-G) particles could be observed during the time-lapse (**Figure 7C-D**). These results indicated that DiD was present in the viral membranes at self-quenching concentrations that could dequench upon lipid mixing. Therefore, the labeled viral preparation could be used to monitor viral fusion.

Figure 7. Characterization of FMT and FMT-(MRB-G) indirectly labeled with DiD. (A) Vero cells were labeled with DiD (DiD+) or PBS (DiD-) for the unlabeled control. Labeled and unlabeled cells were then infected with FMT, FMT-(MRB-G), or PBS for the uninfected control. After cell rounding was observed in infected samples, virus-containing supernatant was collected, filtered, and titred. To test for labeling, U343 cells were bound with supernatant from DiD-labeled veros infected with FMT, FMT-(MRB-G), or PBS (uninfected control) at MOI 50. Nuclei of cells were stained with DAPI. Confocal images were taken in the Alexa-647 channel (DiD) or the DAPI channel (nuclei). (B) Titres of all supernatants. N = 2 biological replicates. (C) Time-lapse images of a DiD-labeled FMT-(MRB-G) particle during a dequenching event in U343 cells. Images of the framed particle are enlarged in the bottom three images. (D) Intensity trace for the particle framed in (C).

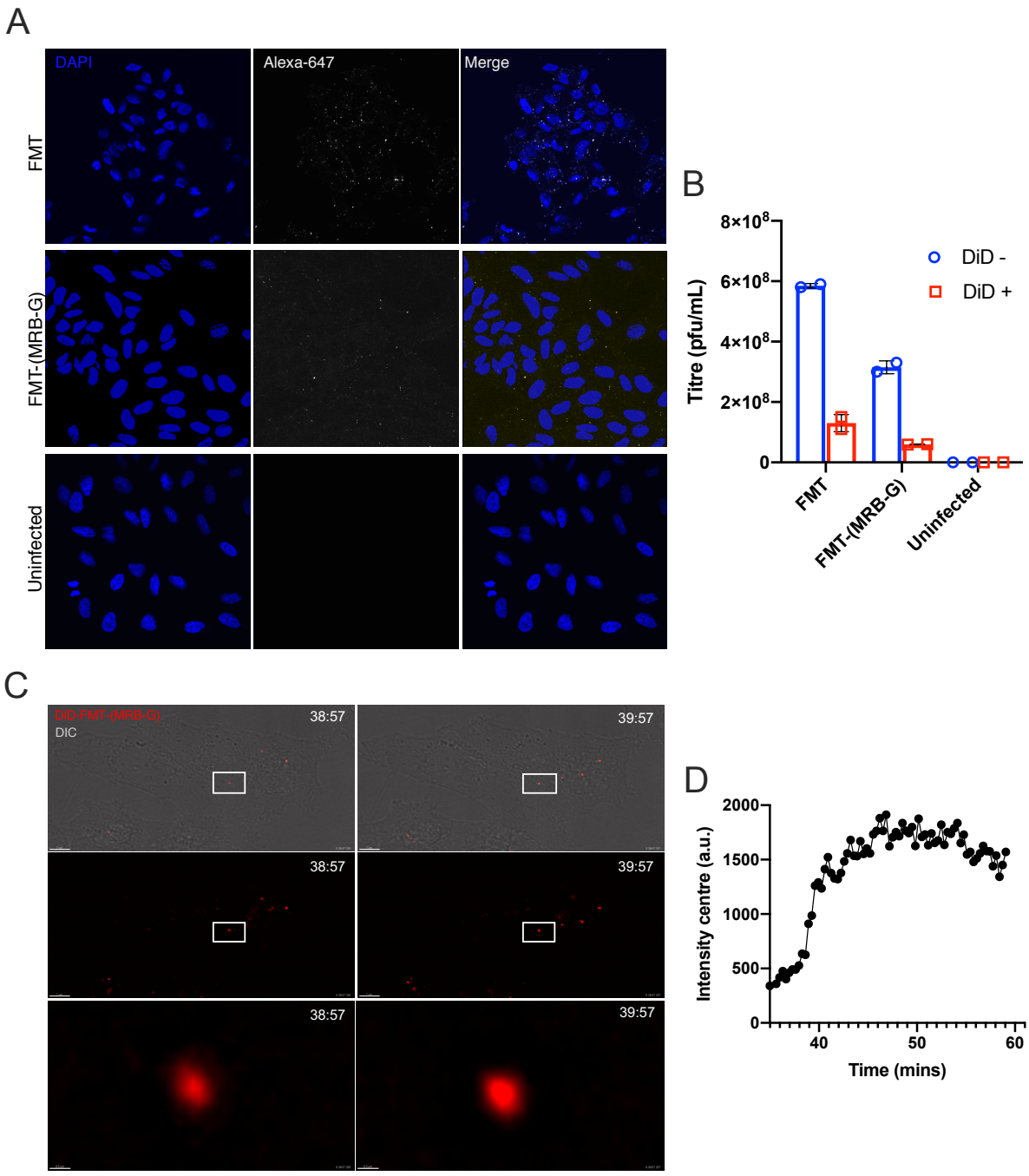
A
DAPI
Alexa-647
Merge
FMT
FMT-(MRB-G)
Uninfected
B
8×10^8
6×10^8
4×10^8
2×10^8
0
Titre (pfu/mL)
DiD -
DiD +
FMT
FMT-(MRB-G)
Uninfected
C
DiD-FMT-(MRB-G)
DIC
38:57
39:57
38:57
39:57
38:57
39:57
D
2000
1500
1000
500
0
Intensity centre (a.u.)
40
50
60
Time (mins)

3.8 Viral fusion of FMT and FMT-(MRB-G) in NHA and U343 cells

Next, viral fusion of DiD-labeled FMT and FMT-(MRB-G) was quantified in NHA and U343 cells via the lipid mixing assay (**Figure 8A, B**). In this assay, the DiD intensity of individual labeled viruses was monitored over the course of an hour. An R script was then used to quantify the percentage of particles that underwent dequenching. As well, the location of FMT and FMT-(MRB-G) viral fusion was determined by colocalizing dequenching particles with endosomal markers.

Imaging revealed that the majority of particles did not undergo lipid mixing in all samples, as observed in previous studies [91,92,124]. Interestingly, only 6% of FMT particles underwent dequenching in astrocytes, whereas 16% of FMT particles dequenched in U343 cells. This suggested that FMT's viral fusion step was attenuated in astrocytes compared to U343 cells. In contrast, 19% of FMT-(MRB-G) particles underwent dequenching in astrocytes and 24% of particles dequenched in U343 cells. This suggested that viral fusion of FMT-(MRB-G) in both astrocytes and U343 cells occurred at similar levels to FMT in U343 cells. Therefore, higher levels of viral fusion were correlated with successful viral infection. Consequently, FMT's attenuated infection in astrocytes could be due to its lower capacity to undergo viral fusion in these cells. As well, FMT fusion appears to occur more efficiently in U343 cells relative to astrocytes. Therefore, the differential in FMT's selectivity for U343 cells compared to astrocytes could be due to differences in the efficiency of viral fusion.

We next sought to determine where FMT fusion occurred in both NHA and U343 cells. Our drug inhibitor experiment in U343 cells suggested that FMT may fuse within endosomes or lysosomes. To further explore this hypothesis, dequenching virions were

colocalized with fluorescently-labeled endosomal markers, including the early endosomal marker EEA1 [125], the late endosomal marker Rab7 [126], and the lysosomal associated membrane protein LAMP1 [127] (**Figure 8C, D**). On average, 79% and 87% of FMT particles dequenched in LAMP1-positive compartments in astrocytes and U343 cells, respectively. This suggested that FMT primarily fuses within lysosomes in both cell lines. Additionally, about 74% and 56% of FMT-(MRB-G) particles dequenched in Rab7-positive compartments in astrocytes and U343 cells, respectively. As well, approximately 34% and 25% of FMT-(MRB-G) particles dequenched within EEA1-positive endosomes in NHA and U343 cells, respectively. This indicated that FMT-(MRB-G) primarily fuses within late endosomes, with minimal fusion occurring in early endosomes. Altogether, these results correlated well with the data from the drug inhibitor experiment, which suggested that FMT fused in a more acidic compartment than FMT-(MRB-G).

Figure 8. Characterizing viral fusion of DiD-labeled FMT and FMT-(MRB-G) in NHA and U343 cells. NHA and U343 cells were infected with DiD-labeled FMT or FMT-(MRB-G) at MOI 100. Images were taken every 20 seconds in the DIC and Cy5 channels with an epifluorescent live cell microscope for 1 hour. (A) Percentage of imaged particles that underwent dequenching. Individual particle intensities were tracked over time with Imaris software. Dequenching events were quantified via R script analysis. Statistics: one-way ANOVA ($F(3, 7) = 20.51$, $p = 0.0008$). Tukey's post hoc test for multiple comparisons: ** = very significant, * = significant (comparing FMT in NHA to FMT in U343 or FMT-(MRB-G) in NHA). N = 3 technical replicates. (B) Images of cells infected with DiD-labeled particles at beginning and end of time-lapse. (C) Colocalization of DiD-labeled FMT or FMT-(MRB-G) with endosomal markers in NHA and U343 cells. NHA and U343 cells were transduced with Cell Light vectors expressing EEA1-eGFP, Rab7-eGFP, or LAMP1-eGFP. Cells were infected with DiD-labeled FMT or FMT-(MRB-G), then imaged as previously described with additional images taken in the FITC channel. Images represent particles colocalizing with endosomal markers during dequenching. (D) Percentage of dequenching particles that colocalized with endosomal markers. N = 3 technical replicates. Data in all figures represents group means +/- SD.

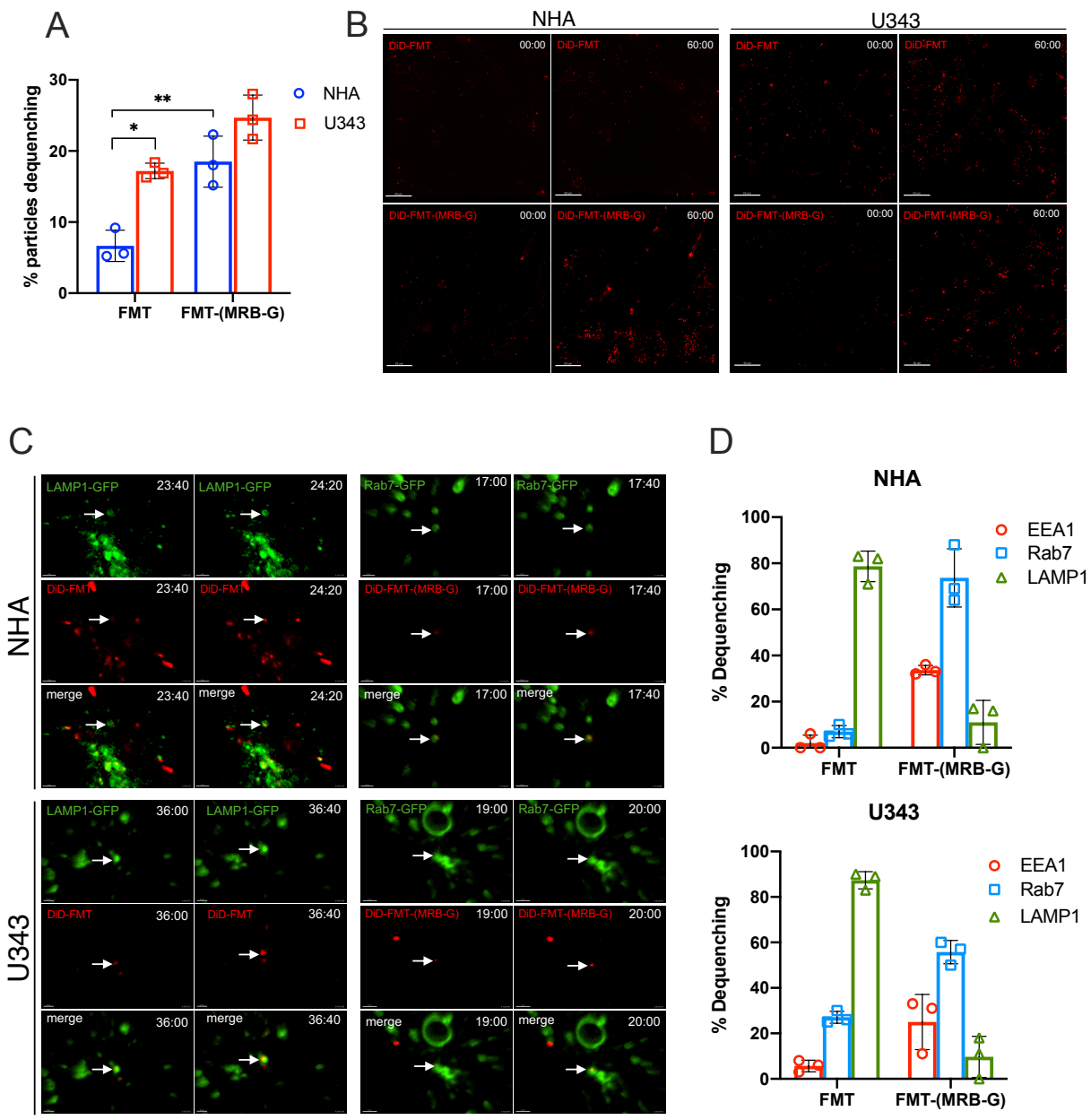
A
% particles dequenching
30
20
10
0
**
*
NHA
U343
FMT
FMT-(MRB-G)
B
NHA
U343
DiD-FMT
00:00
60:00
DiD-FMT-(MRB-G)
C
NHA
U343
LAMP1-GFP
23:40
24:20
36:00
36:40
Rab7-GFP
17:00
17:40
19:00
20:00
DiD-FMT
merge
D
NHA
U343
% Dequenching
100
80
60
40
20
0
EEA1
Rab7
LAMP1
FMT
FMT-(MRB-G)

4. DISCUSSION

GBM is one of the deadliest forms of brain cancer. With a prognosis of 1 to 2 years with current treatment [43], novel therapies for treating this disease are greatly needed. A number of oncolytic viruses with specific tropism for brain cancer cells are currently in development for the treatment of GBM [76,77,128,129]. As intracranial injection is an attractive route of administration for OVs in treating GBM [7,44,45], identifying OVs that balance neurosafety and oncotropism is critical. One OV that achieves this balance is the oncolytic rhabdovirus known as the Farmington virus (FMT). However, the biological mechanisms behind FMT's neurosafety and oncotropism were previously elusive.

Our laboratory had demonstrated FMT's neurosafety in both mice and nonhuman primates. However, we had not investigated the factors underlying this unique neurosafe profile. Our preliminary data suggested that FMT's neurosafety may partially depend on an attenuated capacity to infect normal brain cells. We suspected this attenuation may depend on two main factors: the type 1 IFN response, and the FMT glycoprotein. As we had characterized the IFN-dependent restriction of FMT infection in fibroblasts, we predicted that FMT's attenuated infection in normal brain cells would be IFN-dependent. Additionally, we anticipated that the FMT glycoprotein would restrict FMT infection in brain cells as well. Our studies comparing FMT and MRB pseudotypes conveyed that the MRB glycoprotein was neurotropic, whereas the FMT glycoprotein was not. However, there appeared to be no differential in the infectivity of FMT and MRB in brain tumour cells. As viral entry is a glycoprotein-dependent step that dictates tropism, we suspected that viral entry mediated by the FMT glycoprotein would be less effective than with the MRB glycoprotein. As well, we suspected that viral entry

mediated by either glycoprotein would proceed at similarly high levels in brain cancer cells. Therefore, we hypothesized that FMT's balance of oncotropism and neurosafety was dependent on its distinct tropism for brain tumour cells relative to normal brain cells, which was influenced by the IFN response and the FMT glycoprotein. The defined study set out to investigate the contributions of the IFN response and the FMT glycoprotein in FMT's unique neurosafe and oncotropic profile.

4.1 Neurotropism in mouse neurons

Numerous studies have demonstrated a distinct correlation between neurotoxicity and neurotropism of OVs [61–63,76,77]. Therefore, we predicted that FMT's neurosafety would be similarly correlated with an attenuated capacity to infect normal brain cells. To validate this concept, we examined the infectivity of FMT in mouse neurons and BBB endothelial cells *in vitro,* using the neurotoxic viruses MRB, VSV, and VSVΔ51 as positive controls for neuronal infection. We also tested the infectivity of the FMT variant pseudotyped with MRB, FMT-(MRB-G), as well. Our preliminary data with this virus demonstrated that FMT-(MRB-G) was neurotoxic *in vivo*, whereas a MRB variant pseudotyped with the FMT glycoprotein, MRB-(FMT-G), was neurosafe. This suggested that the MRB glycoprotein was neurotropic whereas the FMT glycoprotein was not. As FMT-(MRB-G) was neurotoxic, we expected this virus to be neurotropic. To test the neurovirulence of these viruses, eGFP-expressing versions of the aforementioned viruses were used as eGFP expression could serve as a marker for positive infection [130].

FMT infection was attenuated in all neuronal populations. As previously described for several neurosafe OVs [76,77], FMT's neuroattenuation correlated well with

its neurosafe profile *in vivo*. Its neuroattenuation also correlated with our preliminary data demonstrating a lack of FMT antigen present within mouse brain sections after IC injection with FMT. While our *in vivo* data has demonstrated that FMT extends survival in mouse models of GBM, we have not characterized FMT's capacity to infect neurons in the presence of a GBM tumour *in vivo*. The GBM tumour microenvironment is known to influence cytokine signaling as well as mediate immune cell populations within the brain [131–133]. Therefore, FMT's infectivity in normal brain tissue could be characterized in mouse models of GBM to account for these additional factors.

FMT infection was attenuated in BBB endothelial cells as well. These cells are known to produce type 1 IFN in response to viral infection [134], which could act as a protective mechanism against FMT. However, this result does not reflect FMT's capacity to pass the BBB *in vivo*. There are a number of unique mechanisms pertaining to the BBB that inhibit viral entry into the brain, such as the presence of tight intercellular junctions that restrict viral passage [135]. Thus, investigating FMT infection of the BBB *in vivo* could help elucidate the mechanisms behind FMT entry into the brain during intravenous administration.

Both wildtype VSV and MRB infected all neuronal populations and BBB endothelial cells. This neurovirulence correlated well with their neurotoxic profiles *in vivo* [60–63]. As well, the neurotropism of the VSV glycoprotein has been well-characterized, and several studies have suggested that the MRB glycoprotein is similarly neurotropic [68]. Both viruses are also capable of restricting the type 1 IFN response and host gene transcription within normal cells, which likely enhanced their ability to infect these cells [60,64–67]. Despite its sensitivity to IFN, VSVΔ51 infected all neuronal populations as well.

This correlated well with its neurotoxicity observed in mice [55,72]. While this virus is more IFN-sensitive than its wildtype counterpart, several studies have demonstrated that IFN production, the IFN response, and basal ISG expression is restricted in neurons relative to other tissues [136–138]. Therefore, the restricted nature of the IFN response within neurons may increase their susceptibility to this IFN-sensitive virus. In addition, VSVΔ51 uses the neurotropic VSV glycoprotein to enter these cells; therefore, it is likely that this virus does not have a barrier to entry. In contrast, VSVΔ51 infection was attenuated within BBB endothelial cells. While VSV may be able to enter these cells, IFN production and the IFN response is higher in BBB endothelial cells compared to neurons [87,100]. Therefore, this more active IFN response may restrict infection and viral spreading of VSVΔ51 within BBB endothelial cells.

FMT-(MRB-G) infected all neurons and BBB endothelial cells as well, which correlated well with its neurotoxic profile. However, our laboratory did not have immunostaining results to demonstrate if this virus could infect normal brain cells *in vivo*, which could further emphasize the link between neurotoxicity and neurovirulence. Interestingly, FMT-(MRB-G) produced interferon in astrocytes. Unfortunately, we did not evaluate if IFN signaling could limit FMT-(MRB-G) infection within neurons. However, we demonstrated that *Ifnb1* expression was delayed in FMT-(MRB-G)-infected astrocytes relative to FMT. This delayed expression of IFN may allow the virus enough time to replicate and spread before the IFN response can exert its effects in neurons. The similar neurovirulence profile of MRB and FMT-(MRB-G) suggested that the MRB glycoprotein is neurotropic, as implied by Brun *et al.* [60]. As well, the differential in neurovirulence between FMT-(MRB-G) and FMT suggested that the FMT glycoprotein

was not neurotropic. Testing the neurovirulence of MRB-(FMT-G) could help validate the neuroattenuated nature of the FMT glycoprotein.

While neuroattenuation is likely an important factor in FMT's neurosafety, there may be additional factors affecting its neurosafety that are independent of neurotropism. For example, the level of inflammation within the brain induced by OV treatment can affect neurosafety as well. The release of DAMPs during tumour cell lysis and the production of proinflammatory cytokines such as IFN can cause an inflammatory response within the brain [51,52]. While a certain level of inflammation is beneficial to tumour reduction, excess inflammation within the brain can cause damage to healthy brain tissues, encephalitis, edema, and even death [139,140]. Oncolytic herpes simplex virus is neuroattenuated, yet IC injection of higher doses of this virus can induce vascular leakage and fatal edema within the brain due to excess inflammation [51]. As well, in a recent clinical trial using a neuroattenuated oncolytic poliovirus to treat GBM, a number of patients experienced adverse neurological symptoms caused by inflammation within the brain in a dose-dependent manner [141]. Similarly, our *in vivo* studies have demonstrated that IC doses of FMT above 1E7 plaque forming units decreased survival in mice. While the cause of this phenomenon has not been studied, the decreased survival is more likely due to excess inflammation caused by FMT, and less likely because of increased viremia. Further studies characterizing the inflammation within the brain with increasing doses of FMT could help elucidate the impact of inflammation in FMT's neurosafety.

4.2 Viral entry

4.2.1 Viral transcript abundance in non-cancerous and cancerous brain cells

Our neurovirulence experiment demonstrated that FMT infection was attenuated relative to FMT-(MRB-G), suggesting that this differential was glycoprotein-dependent. As viral entry is a glycoprotein-mediated process [30], we suspected that FMT infection in normal brain cells may be restricted at the level of viral entry. In contrast, we predicted that FMT-(MRB-G)'s viral entry would be less restricted in these cells. As FMT is a rhabdovirus, we assumed that viral mRNA transcription would be the first step following viral entry [101]. Therefore, if FMT's viral entry was inhibited, viral transcript abundance would be attenuated. To confirm the notion that FMT infection was inhibited at the level of viral entry, we examined the abundance of viral transcripts in FMT-eGFP- and FMT-(MRB-G)-eGFP-infected astrocytes at an MOI of 5. This MOI was used to ensure that cells were saturated with virus, so that each cell would be infected with at least one infectious particle [142]. We predicted that viral transcript abundance would be lower in FMT-eGFP-infected astrocytes compared to FMT-(MRB-G)-eGFP-infected cells. As well, we monitored eGFP levels within infected cells in parallel to monitor the level of infection.

Indeed, FMT-eGFP-infected astrocytes had attenuated viral transcript levels relative to FMT-(MRB-G)-eGFP. eGFP levels also correlated well with viral transcript levels, with fewer GFP-positive cells in FMT-eGFP-infected astrocytes compared to FMT-(MRB-G)-eGFP. The lack of viral transcripts in FMT-eGFP-infected astrocytes could indicate that the viral genome did not enter the cytoplasm successfully [106], which could suggest restricted viral entry. One study also correlated reduced viral mRNA

accumulation with restricted viral entry of VSV in cells expressing IFITM3 [142]. Alternatively, viral transcripts could be degraded by IFN-dependent cellular RNases, such as RNase L [143]. However, the glycoprotein-dependent nature of the differential in viral transcript abundance suggested that FMT infection was restricted at the level of viral entry.

As this experiment suggested that FMT-eGFP viral entry was blocked in astrocytes relative to FMT-(MRB-G)-eGFP, we chose to examine the viral entry of these two viruses in brain cancer cells as well. Brun *et al*. demonstrated that FMT and MRB were highly lytic on 100% of the human brain cancer cell lines tested [60]. This could suggest that the efficiency of viral entry mediated by the FMT glycoprotein may be similar to that of the MRB glycoprotein in brain cancer cells. Therefore, we would expect that the glycoprotein-dependent differential between FMT-eGFP and FMT-(MRB-G)-eGFP would disappear in brain cancer cells. To test this, we evaluated the viral transcript abundance and eGFP expression of FMT-eGFP versus FMT-(MRB-G)-eGFP in the glioblastoma cell line U343.

As expected, FMT-eGFP's infectivity was greater in U343 cells than astrocytes or neurons, confirming FMT's tropism for brain cancer cells. This could suggest that the FMT glycoprotein mediates more effective viral entry into U343 cells compared to NHA cells. FMT's oncotropism also echoed the selectivity of the VSV variants pseudotyped with the LCMV or LASV glycoproteins [76,77]. As well, our results demonstrated that FMT-eGFP and FMT-(MRB-G)-eGFP had very similar transcription and eGFP expression kinetics in U343 cells. Therefore, the glycoprotein-dependent differential in infectivity between FMT-eGFP and FMT-(MRB-G)-eGFP was not present in U343 cells. This

could indicate that viral entry mediated by the FMT glycoprotein and the MRB glycoprotein is similarly efficient in U343 cells.

4.2.2 Viral attachment

Increased viral attachment is often correlated with greater infectivity [33]. As viral attachment is a glycoprotein-dependent step [30], it is feasible that the differential in infectivity between FMT and FMT-(MRB-G) in astrocytes could be due to differences in their binding capacities. The degree of viral attachment is dictated by interactions between the glycoprotein and the viral entry receptor [144]. VSV is known to use the ubiquitously expressed low-density lipoprotein receptor (LDLR) as its primary viral entry receptor [73]. Preliminary data from our laboratory and Doug Mahoney's laboratory has suggested that FMT and MRB both use LDLR to enter cancer cells. LDLR is known to be expressed in U343 cells [145], neurons, and astrocytes [146]. However, due to the complexity of viral attachment [147–149], interactions with the LDLR receptor may differ between the FMT and MRB glycoproteins, and they may also differ between cancer cells and normal cells. It is therefore feasible that the infectivity of FMT and FMT-(MRB-G) in cancerous and non-cancerous brain cells may be influenced by the degree of viral attachment.

Our previous results implied that infection mediated by the FMT glycoprotein may be less effective compared to the MRB glycoprotein in astrocytes. Therefore, we chose to explore the possibility that the FMT glycoprotein may bind astrocytes less efficiently than the MRB glycoprotein. Our results also suggested that the FMT glycoprotein and MRB glycoprotein may mediate similar levels of viral entry in U343 cells. Thus, we predicted that FMT and FMT-(MRB-G) would have similar levels of viral attachment in

U343 cells. To test this, we evaluated the viral attachment of FMT-eGFP and FMT-(MRB-G)-eGFP in U343 and NHA cells via qPCR and microscopy.

Our qPCR results suggested that viral attachment of FMT-eGFP was about 2-3-fold lower than FMT-(MRB-G)-eGFP in NHA cells. Our microscopy images revealed that less FMT-eGFP virions were bound to NHA cells compared to FMT-(MRB-G)-eGFP as well. Interestingly, the qPCR data implied that viral attachment of FMT-eGFP was about 4-fold lower than FMT-(MRB-G)-eGFP in U343 cells as well, which was similarly demonstrated in the microscopy images. Thus, this experiment demonstrated a differential in the viral attachment of the FMT glycoprotein compared to the MRB glycoprotein in both cell lines. The differential in viral attachment between FMT-eGFP and FMT-(MRB-G)-eGFP was unexpected, as these two viruses both infect U343 cells successfully. However, it has been suggested that viruses can infect cells as long as they meet the minimum threshold of viral attachment [33]. Therefore, we can assume that the MRB and FMT glycoproteins both mediated sufficient levels of binding to infect U343 cells. This tropism for brain cancer cells has been previously suggested by Brun *et al.* [60]. As well, our results suggested that the MRB glycoprotein mediated sufficient binding to infect NHA cells as well, which was previously implied by MRB and MRB MG1's tropism for tissues of the CNS [60].

The differential in FMT's tropism for U343 cells relative to NHA cells could be explained by a difference in viral attachment. Cancer cells, including U343 cells, often have upregulated expression of LDLR on their cell membranes as this protein can enhance proliferation and migration of tumour cells [150,151]. Therefore, higher expression of LDLR on U343 cells could increase the number of FMT glycoprotein-LDLR

interactions, thus mediating greater viral attachment and infectivity in U343 cells compared to astrocytes. Additionally, LDLR glycosylation patterns can differ between cancerous and non-cancerous cells [152]. Thus, the binding affinity of the FMT glycoprotein to the LDLR receptor may be higher in U343 cells due to the presence of a glycosylation pattern required for the interaction. While VSV uses LDLR to enter cells, it has been suggested that the proteins phosphatidylserine, sialoglycolipids, or heparan sulfate may act as coreceptors for VSV entry as well [153–155]. Thus, NHA cells may lack a potential coreceptor required for FMT attachment that is present in U343 cells.

Our results suggested that viral attachment mediated by the FMT glycoprotein was lower than with the MRB glycoprotein in both cell lines. However, this experiment did not allow us to determine if the level of FMT attachment we had observed was due to background levels of binding. This could have been achieved by using a negative control virus that could not attach to NHA cells. The level of viral attachment of this negative control virus would then be used to determine the background level of viral attachment at various MOI's. If the level of FMT attachment was below this background level of binding, we could therefore assume that FMT does not attach to NHA cells.

4.2.3 pH-dependent viral fusion

Viral fusion is a glycoprotein-mediated step in viral entry. After viral attachment, viruses can either fuse at the plasma membrane or within intracellular vesicles such as endosomes [30]. In the presence of specific environmental cues, the viral glycoprotein undergoes a conformational change, triggering the fusion of the viral membrane and the host membrane [144]. This then allows the release of the viral genome into the host cell to begin viral replication. Antiviral proteins or host degradation pathways can restrict viral

fusion, thus inhibiting successful viral infection [107–109]. As a glycoprotein-mediated step, we therefore explored the possibility that FMT fusion was restricted in astrocytes relative to U343 cells. We also sought to determine if FMT fusion would be attenuated relative to FMT-(MRB-G) in astrocytes.

In order to explore viral fusion of FMT and FMT-(MRB-G), we first needed to determine where FMT and FMT-(MRB-G) viral fusion occurred within the host cell. Rhabdoviruses such as VSV typically enter cells via endocytosis, and therefore fuse in endosomes [156]. VSV is known to fuse in early or late endosomes, and its fusion is triggered by low pH [157,158]. As FMT and MRB are both rhabdoviruses, we suspected that viral fusion mediated by the FMT and MRB glycoproteins would also be triggered by low pH in endosomes. To evaluate this, we tested the sensitivity of FMT-eGFP, FMT-(MRB-G)-eGFP, MRB-eGFP, and VSV-eGFP infection to various endosomal acidification drug inhibitors, such as bafilomycin B1, ammonium chloride (NH4Cl), and chloroquine in U343 cells. We also tested the sensitivity of VACV-eGFP infection to the drug inhibitors as a potential negative control, as vaccinia virus fusion can be either pH-independent or pH-dependent [116,117].

As expected, the infection of VSV-eGFP in U343 cells was inhibited in a dose-dependent manner by all three drugs. This was consistent with data from several studies demonstrating the sensitivity of VSV infection to bafilomycin, ammonium chloride, and chloroquine [159,160]. MRB-eGFP and FMT-(MRB-G)-eGFP were also similarly inhibited by the three drugs. This implied that viral fusion mediated by the MRB and VSV glycoproteins was triggered by endosome acidification in U343 cells. Thus, VSV-eGFP, MRB-eGFP, and FMT-(MRB-G)-eGFP likely fused within early or late

endosomes, as described for VSV in the literature [157,158]. FMT-eGFP infection was inhibited by bafilomycin and NH4Cl in a dose-dependent manner as well, yet its infection was less sensitive to the drugs than VSV-eGFP, MRB-eGFP, and FMT-(MRB-G)-eGFP. As well, FMT-eGFP infection was not inhibited by chloroquine at any dose. Its sensitivity to bafilomycin and NH4Cl suggested that FMT fusion was triggered by endosomal acidification within U343 cells. However, its lower sensitivity to these drugs and to chloroquine could indicate that FMT fuses in a more acidic compartment than MRB or VSV. More acidic vesicles such as lysosomes may require more drug to neutralize their extremely low pH. As well, lower sensitivity to endosome acidification drug inhibitors has been demonstrated for coronaviruses. Viral fusion of coronaviruses occurs in lysosomes, and its infection was found to be less sensitive to bafilomycin, chloroquine, and NH4Cl compared to VSV [118]. Thus, FMT may fuse in lysosomes in a pH-dependent manner. VACV-eGFP was sensitive to all three drugs, yet its infection was less sensitive than the other viruses tested. Thus, it is likely that VACV-eGFP fuses in endosomes in a pH-dependent manner as well, as has been demonstrated in the literature in several cell lines [161,162]. Thus, the lack of a true negative control in this experiment could not eliminate the possibility that FMT viral fusion occurred in a pH-independent manner. Measles virus, which typically fuses in a pH-independent manner at the plasma membrane, has been found to be insensitive to endosome acidification drug inhibitors [163]. Comparing the sensitivity of FMT and measles infection to these drugs could help eliminate the possibility of a pH-independent mechanism of viral fusion for FMT.

4.2.4 Quantitation of viral fusion

Our drug inhibitor experiment suggested that FMT fuses within lysosomes, and that FMT-(MRB-G) fuses within early or late endosomes. This directed us to choose an assay that could quantify viral fusion levels within the endolysosomal system and simultaneously elucidate the intracellular location of viral fusion. A lipid mixing assay is a well-characterized technique that can be used to quantify viral fusion levels, and can determine the location of viral fusion within endosomes or lysosomes [91,92,119,120,124]. Thus, we used a lipid mixing assay to compare the viral fusion levels of FMT and FMT-(MRB-G) in NHA and U343 cells. We predicted that FMT fusion would be restricted in astrocytes relative to U343 cells. As well, we hypothesized that FMT fusion levels would be attenuated relative to FMT-(MRB-G) in astrocytes. To perform this assay, FMT and FMT-(MRB-G) particles were indirectly labeled with the self-quenching fluorescent dye DiD. NHA and U343 cells were then infected with the labeled particles, and the DiD fluorescence intensity of the virions was monitored over time using time-lapse fluorescence microscopy. The “dequenching” or lipid mixing fusion events were quantified using an R script. To determine the location of FMT and FMT-(MRB-G) viral fusion, we colocalized dequenching virions with the fluorescent endosomal markers EEA1-GFP, Rab7-GFP, or LAMP1-GFP in both cell lines.

As expected, FMT fusion levels in astrocytes were lower than all other samples tested. Only 6% of FMT particles underwent dequenching in astrocytes, whereas 16% of FMT particles dequenched in U343 cells. As well, 19% of FMT-(MRB-G) particles dequenched in NHA cells, and 24% dequenched in U343 cells. These results suggested a correlation between viral fusion levels and infectivity. Indeed, numerous studies have

correlated reduced viral fusion levels with restricted viral infection [92,164,165]. Thus, FMT's restricted levels of viral fusion in astrocytes could limit its infection in these cells. The restriction of FMT fusion within astrocytes could be due to a number of factors. While FMT may use LDLR as its primary cell surface receptor, FMT may require a second intracellular receptor to complete fusion that it cannot bind to in astrocytes. For example, LASV uses α-dystroglycan as its cell surface receptor, and LAMP1 as its intracellular receptor [40]. However, LASV viral fusion is restricted in bird cells due to the absence of a glycosylated residue in LAMP1 required for this interaction [41]. Thus, FMT fusion may be restricted in astrocytes due to poor interactions with a secondary receptor within lysosomes. However, the FMT glycoprotein's interactions with a secondary receptor may be stronger and therefore more effective in U343 cells to mediate fusion.

FMT fusion may also be restricted by the antiviral actions of IFITM proteins. IFITM2 and IFITM3 are localized within late endosomes and lysosomes [39,166]. These proteins can restrict the formation of fusion pores [37] and disrupt endosomal cholesterol homeostasis [39], thus restricting the fusion of several RNA viruses. While the expression of these proteins increases upon IFN signaling, basal levels of these proteins are sufficient to block viral entry in numerous tissues, [34–36], including astrocytes [167]. Thus, it is possible that IFITM proteins restricted FMT fusion within astrocytes.

Interestingly, dequenching FMT particles primarily colocalized with LAMP1-positive vesicles in both NHA and U343 cells. As LAMP1 is a key marker for lysosomes [127], this colocalization indicated that FMT primarily fused within lysosomes in both cell lines. LDLR is known to traffic to lysosomes after internalization [168]; thus, LDLR's interaction with FMT may have helped traffic this virus to the lysosome. As well, our drug inhibitor results indicated that the location of FMT fusion occurred in a more acidic

compartment than FMT-(MRB-G). Indeed, dequenching FMT-(MRB-G) particles primarily colocalized with Rab7-positive vesicles in both cell lines, with some colocalization with EEA1. This suggested that FMT-(MRB-G) primarily fused within late endosomes with minimal fusion in early endosomes. This echoed studies demonstrating VSV viral fusion can occur within early or late endosomes [157,158]. The fact that FMT fused within lysosomes could help explain its restricted fusion in astrocytes. A recent study demonstrated that the fusion of IFITM3-positive vesicles with influenza- or Ebola virus-bearing endosomes prior to viral fusion increased viral trafficking to lysosomes for degradation, thus restricting their infection [92]. As well, IFITM3 coating of lysosomes bearing influenza particles is thought to restrict influenza's viral fusion as well [169]. Thus, it is possible that IFITM3 proteins in astrocytes restricted FMT fusion in lysosomes or led to its degradation in these vesicles. In contrast, viruses that are not restricted by IFITM3 proteins have been shown to fuse before interacting with IFITM3. LASV, an IFITM3-insensitive virus, fuses in late endosomes or lysosomes before colocalizing with IFITM3, thus allowing successful viral fusion and infection [92]. Thus, FMT-(MRB-G) may escape IFITM3-based restriction by fusing before interacting with this antiviral protein. As well, FMT may escape IFITM3 antiviral action in U343 cells, thus allowing its fusion. The impact of IFITM3 proteins on the viral fusion of FMT or FMT-(MRB-G) could be established through colocalizing dequenching and non-dequenching labeled particles with fluorescent IFITM3 proteins.

4.3 The type 1 IFN response

Since our preliminary data suggested that the IFN response restricted FMT infection in fibroblasts, we decided to test the impact of the IFN response on FMT

infection in normal brain cells. We hypothesized that FMT would induce *Ifnb1* and IFNβ1 expression, which would then inhibit its replication cycle. As a negative control for IFN expression, we also characterized the influence of the IFN response on MRB infection as well. As this virus blocks IFN expression [60], we expected to observe low IFN expression from MRB-infected brain cells and little to no inhibition of its replication cycle by IFN-blocking antibodies. Our neuron experiment demonstrated that FMT-(MRB-G) was more neurovirulent than FMT, which could suggest that the MRB glycoprotein is more neurotropic than the FMT glycoprotein. However, we chose to explore the possibility that the induction of IFN expression was glycoprotein-dependent. Studies have demonstrated that certain viral glycoproteins can induce the IFN response through interactions with toll-like receptors during viral attachment or endocytosis, thus restricting infection early on in the replication cycle [90,170,171]. Therefore, we examined the IFN response in both FMT-eGFP and FMT-(MRB-G)-eGFP-infected brain cells. We hypothesized that FMT may induce an earlier or more potent IFN response than FMT-(MRB-G) which could possibly restrict FMT infection.

4.3.1 Interferon beta expression and production

Ifnb1 expression was quantified via qPCR in astrocytes infected with FMT-eGFP or FMT-(MRB-G)-eGFP. Interestingly, *Ifnb1* mRNA and FMT N mRNA were both initially observed around 8 hours in FMT-eGFP-infected astrocytes. The similarity in this timing could suggest that the IFN response was initiated by FMT at a step prior to viral transcription. As seen in the literature [90,170,171], the FMT glycoprotein may contain a pathogen-associated molecular pattern (PAMP) in its sequence that was recognized by the toll-like receptor 4 (TLR4) during viral attachment, thus initiating *Ifnb1* expression.

Alternatively, the FMT genome may have interacted with PRRs during viral entry. The toll-like receptor 7, TLR7, recognizes ssRNA viral genomes [172]. One group found that TLR7 recognition of dengue virus and influenza virus was linked to viral fusion in endosomes [173]. It is therefore possible that viral fusion mediated by the FMT glycoprotein may mediate interactions with TLR7 that could induce IFN expression.

In contrast, *Ifnb1* mRNA expression occurred 8 hours after FMT N mRNA was first observed in FMT-(MRB-G)-eGFP-infected astrocytes. This could suggest that the IFN response was initiated during viral transcription in FMT-(MRB-G)-infected astrocytes. The PRR retinoic-acid-inducible gene 1 (RIG-1) is known to recognize RNA viral genomes in human astrocytes [174]. Therefore, FMT-(MRB-G) viral RNA may have initiated the IFN response through interactions with RIG-1. FMT-(MRB-G)'s late initiation of *Ifnb1* may also suggest that this virus escaped PRR-dependent recognition during viral entry. It is possible that the MRB glycoprotein sequence does not contain the correct PAMPs for TLR-dependent recognition during viral entry. Alternatively, the MRB glycoprotein may inhibit the IFN response directly or indirectly in the early stages of infection. There are several examples of viral proteins that inhibit various aspects of the IFN response. For example, the Yaba-like disease virus secretes a glycoprotein known as Y136 which can bind and inhibit type 1 IFNs [175]. Similarly, the Ebola viral protein VP35 antagonizes the RIG-1-like receptor pathway and binds immunostimulatory viral and host RNAs, thus inhibiting the initiation of the interferon response [176]. Therefore, the MRB glycoprotein may similarly inhibit IFN expression in astrocytes.

As expected, MRB-eGFP-infected astrocytes secreted very little IFNβ1, which was likely a result of the inhibition of IFN expression by the MRB matrix protein [60]. In contrast,

IFNβ1 was secreted by both FMT-eGFP- and FMT-(MRB-G)-eGFP-infected astrocytes at 24 hours post-infection. This correlated with the detection of *Ifnb1* mRNA at 24 hours, and with the high capacity of astrocytes to produce IFNβ1 in response to RNA virus infection [177]. High expression of IFNβ1 in astrocytes is essential to protecting brain tissues from infection, and to the maintenance of BBB structural integrity [87]. Therefore, FMT's ability to induce IFNβ1 expression in astrocytes may play a key role in FMT's neurosafety. Unfortunately, the level of IFNβ1 produced in response to the two viruses was higher than the maximum detection level of the ELISA kit. Therefore, the exact concentration of IFNβ1 produced in response to FMT versus FMT-(MRB-G) was unknown. Determining this concentration of IFNβ1 could elucidate a differential in the levels of IFNβ1 produced by the two viruses, which could potentially explain their different levels of infection in astrocytes. As well, correlating IFNβ1 levels to *Ifnb1* mRNA levels at different timepoints post-infection could support the concept of glycoprotein-dependent IFN expression.

Overall, these results suggested that FMT and FMT-(MRB-G) both produced IFN in astrocytes. The differential in the initiation of *Ifnb1* expression with FMT versus FMT-(MRB-G) could affect the infectivity of these two viruses in brain cells. The glycoprotein-dependent initiation of IFN expression could be further characterized through the use of virus-like particles (VLPs) pseudotyped with the FMT or MRB glycoprotein, or with the MRB-(FMT-G) virus.

4.3.2 Interferon beta dependent viral restriction

Finally, we studied the effect of IFN signaling on FMT and MRB infection in cortical neurons by blocking IFNβ1 with neutralizing antibodies. As expected, MRB infected neurons in the presence of both anti-IFNβ1 and control antibodies at all concentrations. As

our IFNβ1 ELISA results suggested, MRB likely blocked IFN production upon infection, therefore the antibodies would have no IFNβ1 to block. In contrast, FMT demonstrated minimal infection in neurons in the presence of control antibodies. However, FMT infection increased significantly in the presence of IFNβ1-blocking antibodies. When IFNβ1 is secreted by infected cells, IFNβ1 binds to the IFNAR of both infected and uninfected cells [20,21]. Downstream signaling from this receptor induces the expression of ISGs, which then restrict viral replication at all stages of the replication cycle in both infected and uninfected cells [22,23]. Therefore, IFNβ1-dependent signaling may have induced the expression of various ISGs that then restricted FMT infection within infected and uninfected cells. However, dose-dependent inhibition of FMT infection with the different concentrations of IFNβ1-blocking antibodies was not observed. It is possible that the 4X and 10X concentrations of antibodies both saturated the levels of IFNβ1 present. To truly observe a dose-dependent inhibition of FMT infection, lower concentrations of IFNβ1-blocking antibodies could be used. As well, characterizing the impact of the IFN response on the infection of FMT-(MRB-G) in astrocytes could help to further investigate the glycoprotein-dependent nature of the IFN response.

4.4 Concluding remarks

In this project, we set out to investigate the biological mechanisms underlying FMT's neurosafety and oncotropism. We found that FMT's neurosafety may in part be due to its attenuated infection in both neurons and astrocytes. Our results suggested that a key factor dictating FMT's attenuated infection within normal brain cells was the type 1 IFN response. FMT induced type 1 IFN expression within astrocytes and neurons, and IFN-dependent signaling appeared to restrict FMT infection and spread

within neurons. The FMT glycoprotein may also be an important factor governing FMT's restricted infection within normal brain cells. Our results suggested that FMT was blocked at an early stage of infection within astrocytes, and that this block was glycoprotein-dependent. It appeared that viral binding and fusion in astrocytes mediated by the FMT glycoprotein was less effective relative to neurotropic viruses. Our data also indicated that the FMT glycoprotein played a role in dictating FMT's tropism for brain cancer cells, as the FMT glycoprotein mediated greater levels of viral fusion within brain cancer cells compared to astrocytes.

Our results demonstrated that FMT viral entry in astrocytes may be restricted. However, FMT's viral entry was not characterized within neurons. Our neuron experiment and neurotoxicity *in vivo* data suggested that the FMT glycoprotein may be important for FMT's neuroattenuation. Therefore, similar glycoprotein-dependent mechanisms of restriction may also apply to neurons. Thus, all viral entry experiments should be repeated within neurons to better elucidate this role.

As well, we did not fully determine how the FMT glycoprotein restricted FMT infection within normal brain cells yet mediated successful infection within brain cancer cells. For example, we were not able to determine if the level of FMT viral attachment we observed in astrocytes was above background levels of binding. To determine the background level of viral attachment, the binding of a virus known to not bind astrocytes could be used as a negative control. As well, our experiment could not compare FMT viral binding levels between U343 cells and astrocytes. This could be elucidated through flow cytometry-based assays to better quantify the number of cells as well as the degree of viral binding. While our data demonstrated that FMT fusion was limited in

astrocytes relative to U343 cells, we were not able to elucidate a mechanism behind this restriction. As FMT fused within lysosomes, lysosomal-dependent degradation of FMT particles could be measured as a potential mechanism of restriction within astrocytes. IFITM proteins are also known to restrict viral fusion within normal cells. Therefore, FMT infection could be measured in IFITM knockout cells to elucidate the impact of these antiviral proteins in FMT restriction. Overall, there is a lack of information regarding the host proteins required to mediate successful viral entry of FMT. Therefore, an siRNA screen could be used to determine important factors needed for FMT viral entry.

Our results suggested that IFN signaling restricted FMT infection within neurons. However, this was not proven in astrocytes. Therefore, a similar IFN-neutralization experiment could be performed to elucidate the impact of IFN signaling on FMT infection within astrocytes. As well, our qPCR results suggested that FMT induced *Ifnb1* expression 8 hours earlier than FMT-(MRB-G). This suggested a potential link between the viral glycoprotein and the induction of the IFN response. Potentially, the FMT glycoprotein may interact with various toll-like receptors during viral entry that then trigger the IFN response. These viral glycoprotein-receptor interactions could be tested through the use of VLPs expressing the FMT glycoprotein or with the MRB variant MRB-(FMT-G). Alternatively, the MRB glycoprotein may delay IFN expression within astrocytes. This could be evaluated through challenging cells with IFN-inducing agents such as poly I:C [178], expressing the MRB glycoprotein within cells, and quantifying *Ifnb1* expression.

While our experiments characterized FMT and FMT-(MRB-G) infection in normal brain cells *in vitro*, it is possible that these infection levels may change *in vivo* in the

presence of a GBM tumour. Therefore, characterizing FMT and FMT-(MRB-G) infection within GBM mouse models *in vivo* could help elucidate any changes to tropism. Additionally, FMT-induced inflammation within the brain and its relation to neurosafety has not been fully characterized. Thus, characterizing cytokine and immune populations alongside neurological function within mouse brains post-IC injection with FMT could help elucidate this role.

More experiments are necessary to fully characterize the biological mechanisms underlying FMT's neurosafety and oncotropism. However, this study highlighted the importance of the viral glycoprotein and the type 1 interferon response in dictating this tropism. Further characterizing the virus-host interactions governing the selectivity of OVs is necessary to improve the safety and efficacy of these therapies for the treatment of GBM.

REFERENCES

1. Bray, F. *et al.* Global cancer statistics 2018: GLOBOCAN estimates of incidence and mortality worldwide for 36 cancers in 185 countries1. Bray F, Ferlay J, Soerjomataram I, Siegel RL, Torre LA, Jemal A. Global cancer statistics 2018: GLOBOCAN estimates of incidence and mo. *CA. Cancer J. Clin.* **68**, 394–424 (2018).
2. Falzone, L., Salomone, S. & Libra, M. Evolution of cancer pharmacological treatments at the turn of the third millennium. *Frontiers in Pharmacology* **9**, (2018).
3. Armstrong, D. K. Relapsed Ovarian Cancer: Challenges and Management Strategies for a Chronic Disease. *Oncologist* **7**, 20–28 (2002).
4. Van Der Jeught, K., Xu, H. C., Li, Y. J., Lu, X. Bin & Ji, G. Drug resistance and new therapies in colorectal cancer. *World Journal of Gastroenterology* **24**, 3834–3848 (2018).
5. Gonzalez-Angulo, A. M., Morales-Vasquez, F. & Hortobagyi, G. N. Overview of resistance to systemic therapy in patients with breast cancer. *Adv. Exp. Med. Biol.* **608**, 1–22 (2007).
6. Pikor, L. A., Bell, J. C. & Diallo, J.-S. Oncolytic Viruses: Exploiting Cancer's Deal with the Devil. *Trends in cancer* **1**, 266–277 (2015).
7. Martikainen, M. & Essand, M. Virus-based immunotherapy of glioblastoma. *Cancers* **11**, (2019).
8. Diaz, R. M. *et al.* Oncolytic immunovirotherapy for melanoma using vesicular stomatitis virus. *Cancer Res.* **67**, 2840–8 (2007).
9. Kölmel, K. F. *et al.* Prior immunisation of patients with malignant melanoma with vaccinia or BCG is associated with better survival. An European Organization for Research and Treatment of Cancer cohort study on 542 patients. *Eur. J. Cancer* **41**, 118–25 (2005).
10. Benencia, F., Courrèges, M. C., Fraser, N. W. & Coukos, G. Herpes virus oncolytic therapy reverses tumor immune dysfunction and facilitates tumor antigen presentation. *Cancer Biol. Ther.* **7**, 1194–205 (2008).
11. Prestwich, R. J. *et al.* Reciprocal human dendritic cell-natural killer cell interactions induce antitumor activity following tumor cell infection by oncolytic reovirus. *J. Immunol.* **183**, 4312–21 (2009).
12. Shi, G. *et al.* Modulating the Tumor Microenvironment via Oncolytic Viruses and CSF-1R Inhibition Synergistically Enhances Anti-PD-1 Immunotherapy. *Mol. Ther.* (2019). doi:10.1016/j.ymthe.2018.11.010
13. Ahn, J. B. *et al.* Tumor microenvironment remodeling by intratumoral oncolytic vaccinia virus enhances the efficacy of immune checkpoint blockade. *Clin. Cancer Res.* (2018). doi:10.1158/1078-0432.ccr-18-1932
14. Yin, J., Markert, J. M. & Leavenworth, J. W. Modulation of the Intratumoral Immune Landscape by Oncolytic Herpes Simplex Virus Virotherapy. *Front. Oncol.* (2017). doi:10.3389/fonc.2017.00136
15. Rosenzweig, J. P. *et al.* Oncolytic viruses—interaction of virus and Tumor Cells in the Battle to eliminate Cancer. *Front. Oncol* **7**, 1953389–195 (2017).
16. Jhawar, S. R. *et al.* Oncolytic viruses-natural and genetically engineered cancer

immunotherapies. *Frontiers in Oncology* **7**, (2017).
17. Ivashkiv, L. B. & Donlin, L. T. Regulation of type i interferon responses. *Nature Reviews Immunology* (2014). doi:10.1038/nri3581
18. Paludan, S. & Bowie, A. Immune Sensing of DNA. *Immunity* (2013). doi:10.1016/j.immuni.2013.05.004
19. Goubau, D., Deddouche, S. & Reis e Sousa, C. Cytosolic sensing of viruses. *Immunity* **38**, 855–69 (2013).
20. Nan, Y., Wu, C. & Zhang, Y. J. Interplay between Janus kinase/signal transducer and activator of transcription signaling activated by type I interferons and viral antagonism. *Frontiers in Immunology* (2017). doi:10.3389/fimmu.2017.01758
21. Majoros, A. *et al.* Canonical and non-canonical aspects of JAK-STAT signaling: Lessons from interferons for cytokine responses. *Frontiers in Immunology* (2017). doi:10.3389/fimmu.2017.00029
22. Schneider, W. M., Chevillotte, M. D. & Rice, C. M. Interferon-Stimulated Genes: A Complex Web of Host Defenses. *Annu. Rev. Immunol.* (2014). doi:10.1146/annurev-immunol-032713-120231
23. Schoggins, J. W. Recent advances in antiviral interferon-stimulated gene biology. *F1000Research* (2018). doi:10.12688/f1000research.12450.1
24. Dunn, G. P. *et al.* A critical function for type I interferons in cancer immunoediting. *Nat. Immunol.* **6**, 722–9 (2005).
25. Budczies, J. *et al.* Mutation patterns in genes encoding interferon signaling and antigen presentation: A pan-cancer survey with implications for the use of immune checkpoint inhibitors. *Genes. Chromosomes Cancer* **56**, 651–659 (2017).
26. Stojdl, D. F. *et al.* Exploiting tumor-specific defects in the interferon pathway with a previously unknown oncolytic virus. *Nat. Med.* (2000). doi:10.1038/77558
27. Franco, S. Di, Turdo, A., Todaro, M. & Stassi, G. Role of Type I and II interferons in colorectal cancer and melanoma. *Frontiers in Immunology* **8**, (2017).
28. Katsoulidis, E., Kaur, S. & Platanias, L. C. Deregulation of interferon signaling in malignant cells. *Pharmaceuticals* (2010). doi:10.3390/ph3020406
29. Matveeva, O. V, Peter, | & Chumakov, M. Defects in interferon pathways as potential biomarkers of sensitivity to oncolytic viruses. (2018). doi:10.1002/rmv.2008
30. Cook, J. D. & Lee, J. E. The Secret Life of Viral Entry Glycoproteins: Moonlighting in Immune Evasion. *PLoS Pathog.* **9**, (2013).
31. Bowden, T. A., Jones, E. Y. & Stuart, D. I. Cells under siege: Viral glycoprotein interactions at the cell surface. *Journal of Structural Biology* **175**, 120–126 (2011).
32. Kohlhapp, F. J., Zloza, A. & Kaufman, H. L. Talimogene laherparepvec (T-VEC) as cancer immunotherapy. *Drugs Today (Barc).* **51**, 549–58 (2015).
33. Hasegawa, K. *et al.* Affinity Thresholds for Membrane Fusion Triggering by Viral Glycoproteins. *J. Virol.* (2007). doi:10.1128/jvi.01415-07
34. Siegrist, F., Ebeling, M. & Certa, U. The small interferon-induced transmembrane genes and proteins. *J. Interferon Cytokine Res.* **31**, 183–97 (2011).
35. Monel, B. *et al.* Zika virus induces massive cytoplasmic vacuolization and paraptosis-like death in infected cells. *EMBO J.* **36**, 1653–1668 (2017).
36. Alteber, Z. *et al.* The anti-inflammatory IFITM genes ameliorate colitis and partially protect from tumorigenesis by changing immunity and microbiota. *Immunol. Cell*

Biol. **96**, 284–297 (2018).
37. Desai, T. M. *et al.* IFITM3 Restricts Influenza A Virus Entry by Blocking the Formation of Fusion Pores following Virus-Endosome Hemifusion. *PLoS Pathog.* **10**, e1004048 (2014).
38. Spence, J. S. *et al.* IFITM3 directly engages and shuttles incoming virus particles to lysosomes. *Nat. Chem. Biol.* (2019). doi:10.1038/s41589-018-0213-2
39. Amini-Bavil-Olyaee, S. *et al.* The antiviral effector IFITM3 disrupts intracellular cholesterol homeostasis to block viral entry. *Cell Host Microbe* **13**, 452–64 (2013).
40. Jae, L. T. *et al.* Lassa virus entry requires a trigger-induced receptor switch. *Science (80-.).* **344**, 1506–1510 (2014).
41. Heffernan, M., Yousefi, S. & Dennis, J. W. Molecular Characterization of P2B/LAMP-1, a Major Protein Target of a Metastasis-associated Oligosaccharide Structure. *Cancer Res.* **49**, 6077–6084 (1989).
42. Urbanska, K., Sokolowska, J., Szmidt, M. & Sysa, P. Glioblastoma multiforme - An overview. *Wspolczesna Onkologia* **18**, 307–312 (2014).
43. Stupp, R. *et al.* EORTC 22981: Radiotherapy plus concomitant and adjuvant temozolomide for globlastoma. *N Engl J Med* (2005). doi:10.1016/j.canrad.2005.05.001
44. Wollmann, G., Ozduman, K. & Van Den Pol, A. N. Oncolytic virus therapy for glioblastoma multiforme: Concepts and candidates. *Cancer Journal* **18**, 69–81 (2012).
45. Foreman, P. M., Friedman, G. K., Cassady, K. A. & Markert, J. M. Oncolytic Virotherapy for the Treatment of Malignant Glioma. *Neurotherapeutics* **14**, 333–344 (2017).
46. Ackerman, S. Major Structures and Functions of the Brain. (1992).
47. Muñoz-Elías, G., Woodbury, D. & Black, I. B. Marrow stromal cells, mitosis, and neuronal differentiation: stem cell and precursor functions. *Stem Cells* **21**, 437–48 (2003).
48. van den Pol, A. N. Viral Infection Leading to Brain Dysfunction: More Prevalent Than Appreciated? *Neuron* **64**, 17–20 (2009).
49. Soung, A. & Klein, R. S. Viral Encephalitis and Neurologic Diseases: Focus on Astrocytes. *Trends in Molecular Medicine* **24**, 950–962 (2018).
50. Garber, C. *et al.* Astrocytes decrease adult neurogenesis during virus-induced memory dysfunction via IL-1. *Nat. Immunol.* **19**, 151–161 (2018).
51. Hong, B. *et al.* Suppression of HMGB1 Released in the Glioblastoma Tumor Microenvironment Reduces Tumoral Edema. *Mol. Ther. - Oncolytics* **12**, 93–102 (2019).
52. Yeung, Y. T., McDonald, K. L., Grewal, T. & Munoz, L. Interleukins in glioblastoma pathophysiology: Implications for therapy. *British Journal of Pharmacology* **168**, 591–606 (2013).
53. Venkatesan, A. & Geocadin, R. G. Diagnosis and management of acute encephalitis: A practical approach. *Neurol. Clin. Pract.* **4**, 206–215 (2014).
54. Wollmann, G., Robek, M. D. & van den Pol, A. N. Variable Deficiencies in the Interferon Response Enhance Susceptibility to Vesicular Stomatitis Virus Oncolytic Actions in Glioblastoma Cells but Not in Normal Human Glial Cells. *J. Virol.* (2007). doi:10.1128/jvi.01861-06

55. Lun, X. *et al.* Effects of Intravenously Administered Recombinant Vesicular Stomatitis Virus (VSV ΔM51) on Multifocal and Invasive Gliomas. *JNCI J. Natl. Cancer Inst.* **98**, 1546–1557 (2006).
56. Ozduman, K., Wollmann, G., Piepmeier, J. M. & van den Pol, A. N. Systemic vesicular stomatitis virus selectively destroys multifocal glioma and metastatic carcinoma in brain. *J. Neurosci.* **28**, 1882–93 (2008).
57. Haseley, A. *et al.* Extracellular matrix protein CCN1 limits oncolytic efficacy in glioma. *Cancer Res.* **72**, 1353–62 (2012).
58. Ruotsalainen, J. *et al.* Interferon-B sensitivity of tumor cells correlates with poor response to VA7 virotherapy in mouse glioma models. *Mol. Ther.* (2012). doi:10.1038/mt.2012.53
59. Alain, T. *et al.* Vesicular stomatitis virus oncolysis is potentiated by impairing mTORC1-dependent type I IFN production. *Proc. Natl. Acad. Sci.* (2010). doi:10.1073/pnas.0912344107
60. Brun, J. *et al.* Identification of genetically modified maraba virus as an oncolytic rhabdovirus. *Mol. Ther.* (2010). doi:10.1038/mt.2010.103
61. van den Pol, A. N., Dalton, K. P. & Rose, J. K. Relative neurotropism of a recombinant rhabdovirus expressing a green fluorescent envelope glycoprotein. *J. Virol.* **76**, 1309–27 (2002).
62. Johnson, J. E. *et al.* Neurovirulence properties of recombinant vesicular stomatitis virus vectors in non-human primates. *Virology* **360**, 36–49 (2007).
63. Quiroz, E., Moreno, N., Peralta, P. H. & Tesh, R. B. A human case of encephalitis associated with vesicular stomatitis virus (Indiana serotype) infection. *Am. J. Trop. Med. Hyg.* **39**, 312–4 (1988).
64. Stojdl, D. F. *et al.* VSV strains with defects in their ability to shutdown innate immunity are potent systemic anti-cancer agents. *Cancer Cell* **4**, 263–75 (2003).
65. Wu, L. *et al.* rVSV(M Delta 51)-M3 is an effective and safe oncolytic virus for cancer therapy. *Hum. Gene Ther.* **19**, 635–47 (2008).
66. Goel, A. *et al.* Radioiodide imaging and radiovirotherapy of multiple myeloma using VSV(Δ51)-NIS, an attenuated vesicular stomatitis virus encoding the sodium iodide symporter gene. *Blood* **110**, 2342–2350 (2007).
67. Corredor, J. C. *et al.* N-Myc expression enhances the oncolytic effects of vesicular stomatitis virus in human neuroblastoma cells. *Mol. Ther. - Oncolytics* **3**, 16005 (2016).
68. Pol, J. *et al.* Development and applications of oncolytic Maraba virus vaccines. *Oncolytic Virotherapy* **Volume 7**, 117–128 (2018).
69. Alajez, N. M., Mocanu, J. D., Krushel, T., Bell, J. C. & Liu, F. F. Enhanced vesicular stomatitis virus (VSVΔ51) targeting of head and neck cancer in combination with radiation therapy or ZD6126 vascular disrupting agent. *Cancer Cell Int.* **12**, (2012).
70. Alajez, N. M. *et al.* Efficacy of systemically administered mutant vesicular stomatitis virus (VSVΔ51) combined with radiation for nasopharyngeal carcinoma. *Clin. Cancer Res.* **14**, 4891 (2008).
71. Beug, S. T. *et al.* Combination of IAP Antagonists and TNF-α-Armed Oncolytic Viruses Induce Tumor Vascular Shutdown and Tumor Regression. *Mol. Ther. - Oncolytics* **10**, 28–39 (2018).

72. Ozduman, K., Wollmann, G., Ahmadi, S. A. & van den Pol, A. N. Peripheral Immunization Blocks Lethal Actions of Vesicular Stomatitis Virus within the Brain. *J. Virol.* (2009). doi:10.1128/jvi.02558-08
73. Finkelshtein, D., Werman, A., Novick, D., Barak, S. & Rubinstein, M. LDL receptor and its family members serve as the cellular receptors for vesicular stomatitis virus. *Proc. Natl. Acad. Sci. U. S. A.* **110**, 7306–11 (2013).
74. Tani, H. *et al.* Replication-Competent Recombinant Vesicular Stomatitis Virus Encoding Hepatitis C Virus Envelope Proteins. *J. Virol.* **81**, 8601–8612 (2007).
75. Boritz, E., Gerlach, J., Johnson, J. E. & Rose, J. K. Replication-Competent Rhabdoviruses with Human Immunodeficiency Virus Type 1 Coats and Green Fluorescent Protein: Entry by a pH-Independent Pathway. *J. Virol.* **73**, (1999).
76. Wollmann, G., Drokhlyansky, E., Davis, J. N., Cepko, C. & van den Pol, A. N. Lassa-vesicular stomatitis chimeric virus safely destroys brain tumors. *J. Virol.* **89**, 6711–24 (2015).
77. Ebert, O. *et al.* Re-engineering VSV to Abrogate Neurotoxicity, Circumevent Humoral Immunity and Enhance Oncolytic Potency. *Cancer Res.* (2014). doi:10.1158/0008-5472.can-13-3306
78. Zaccaria, M. L., Di Tommaso, F., Brancaccio, A., Paggi, P. & Petrucci, T. C. Dystroglycan distribution in adult mouse brain: a light and electron microscopy study. *Neuroscience* **104**, 311–24 (2001).
79. Smelt, S. C. *et al.* Differences in Affinity of Binding of Lymphocytic Choriomeningitis Virus Strains to the Cellular Receptor -Dystroglycan Correlate with Viral Tropism and Disease Kinetics. *J. Virol.* **75**, 448–457 (2001).
80. Satz, J. S. *et al.* Distinct functions of glial and neuronal dystroglycan in the developing and adult mouse brain. *J. Neurosci.* **30**, 14560–72 (2010).
81. Kunz, S. *et al.* Posttranslational modification of alpha-dystroglycan, the cellular receptor for arenaviruses, by the glycosyltransferase LARGE is critical for virus binding. *J. Virol.* **79**, 14282–96 (2005).
82. Anderson, B. D., Nakamura, T., Russell, S. J. & Peng, K.-W. High CD46 receptor density determines preferential killing of tumor cells by oncolytic measles virus. *Cancer Res.* **64**, 4919–26 (2004).
83. Palacios, G. *et al.* Characterization of Farmington virus, a novel virus from birds that is distantly related to members of the family Rhabdoviridae. *Virol. J.* **10**, (2013).
84. Marié, I., Durbin, J. E. & Levy, D. E. Differential viral induction of distinct interferon-alpha genes by positive feedback through interferon regulatory factor-7. *EMBO J.* **17**, 6660–9 (1998).
85. Erlandsson, L. *et al. Interferon-beta is required for interferon-alpha production in mouse fibroblasts. Current biology : CB* **8**, (2014).
86. Samuelsson, C. V *et al.* Transformation of mouse fibroblasts alters the induction pattern of type I IFNs after virus infection. *Biochem. Biophys. Res. Commun.* **335**, 584–9 (2005).
87. Daniels, B. P. *et al.* Regional astrocyte IFN signaling restricts pathogenesis during neurotropic viral infection. *J. Clin. Invest.* **127**, 843–856 (2017).
88. Georgel, P. *et al.* Vesicular stomatitis virus glycoprotein G activates a specific antiviral Toll-like receptor 4-dependent pathway. *Virology* **362**, 304–313 (2007).

89. Boehme, K. W. & Compton, T. Innate Sensing of Viruses by Toll-Like Receptors. *J. Virol.* **78**, 7867–7873 (2004).
90. Okumura, A., Pitha, P. M., Yoshimura, A. & Harty, R. N. Interaction between Ebola virus glycoprotein and host toll-like receptor 4 leads to induction of proinflammatory cytokines and SOCS1. *J. Virol.* **84**, 27–33 (2010).
91. Spence, J. S., Krause, T. B., Mittler, E., Jangra, R. K. & Chandran, K. Direct Visualization of Ebola Virus Fusion Triggering in the Endocytic Pathway. *MBio* **7**, e01857-15 (2016).
92. Spence, J. S. *et al.* IFITM3 directly engages and shuttles incoming virus particles to lysosomes. *Nat. Chem. Biol.* **15**, 259–268 (2019).
93. Zhu, Z. *et al.* Zika virus has oncolytic activity against glioblastoma stem cells. *J. Exp. Med.* **214**, 2843–2857 (2017).
94. Samson, A. *et al.* Intravenous delivery of oncolytic reovirus to brain tumor patients immunologically primes for subsequent checkpoint blockade. *Sci. Transl. Med.* **10**, eaam7577 (2018).
95. Wu, Y. *et al.* Oncolytic efficacy of recombinant vesicular stomatitis virus and myxoma virus in experimental models of rhabdoid tumors. *Clin. Cancer Res.* **14**, 1218–27 (2008).
96. Lee, A. S.-Y., Burdeinick-Kerr, R. & Whelan, S. P. J. A genome-wide small interfering RNA screen identifies host factors required for vesicular stomatitis virus infection. *J. Virol.* **88**, 8355–60 (2014).
97. Li, Q. *et al.* A genome-wide genetic screen for host factors required for hepatitis C virus propagation. *Proc. Natl. Acad. Sci. U. S. A.* **106**, 16410–5 (2009).
98. Ehrengruber, M. U. *et al.* Recombinant Semliki Forest virus and Sindbis virus efficiently infect neurons in hippocampal slice cultures. *Proc. Natl. Acad. Sci. U. S. A.* **96**, 7041–6 (1999).
99. Perez, J. T., García-Sastre, A. & Manicassamy, B. Insertion of a GFP Reporter Gene in Influenza Virus. *Curr. Protoc. Microbiol.* **29**, 15G.4.1-15G.4.16 (2013).
100. Sommereyns, C., Paul, S., Staeheli, P. & Michiels, T. IFN-lambda (IFN-λ) is expressed in a tissue-dependent fashion and primarily acts on epithelial cells in vivo. *PLoS Pathog.* **4**, (2008).
101. Carey, B. L., Ahmed, M., Puckett, S. & Lyles, D. S. Early steps of the virus replication cycle are inhibited in prostate cancer cells resistant to oncolytic vesicular stomatitis virus. *J. Virol.* **82**, 12104–15 (2008).
102. Villarreal, L. P., Breindl, M. & Holland, J. J. Determination of molar ratios of vesicular stomatitis virus induced RNA species in BHK $_{21}$ cells. *Biochemistry* **15**, 1663–1667 (1976).
103. Roche, S., Albertini, A. A. V., Lepault, J., Bressanelli, S. & Gaudin, Y. Structures of vesicular stomatitis virus glycoprotein: membrane fusion revisited. *Cell. Mol. Life Sci.* **65**, 1716–1728 (2008).
104. Florkiewicz, R. Z. & Rose, J. K. A cell line expressing vesicular stomatitis virus glycoprotein fuses at low pH. *Science* **225**, 721–3 (1984).
105. Riedel, H., Kondor-Koch, C. & Garoff, H. Cell surface expression of fusogenic vesicular stomatitis virus G protein from cloned cDNA. *EMBO J.* **3**, 1477–83 (1984).
106. Yamauchi, Y. & Helenius, A. Virus entry at a glance. *J. Cell Sci.* (2013).

doi:10.1242/jcs.119685
107. Bailey, C. C., Zhong, G., Huang, I.-C. & Farzan, M. IFITM-Family Proteins: The Cell's First Line of Antiviral Defense. *Annu. Rev. Virol.* (2014). doi:10.1146/annurev-virology-031413-085537
108. Colomer-Lluch, M., Ruiz, A., Moris, A. & Prado, J. G. Restriction Factors: From Intrinsic Viral Restriction to Shaping Cellular Immunity Against HIV-1. *Frontiers in immunology* (2018). doi:10.3389/fimmu.2018.02876
109. Seissler, T., Marquet, R. & Paillart, J. C. Hijacking of the ubiquitin/proteasome pathway by the hiv auxiliary proteins. *Viruses* (2017). doi:10.3390/v9110322
110. Clague, M. J., Schoch, C., Zech, L. & Blumenthal, R. Gating kinetics of pH-activated membrane fusion of vesicular stomatitis virus with cells: stopped-flow measurements by dequenching of octadecylrhodamine fluorescence. *Biochemistry* **29**, 1303–1308 (1990).
111. Benmansour, A., de Kinkelin, P. & Gaudin, Y. Mutations in the glycoprotein of viral haemorrhagic septicaemia virus that affect virulence for fish and the pH threshold for membrane fusion. *J. Gen. Virol.* **80**, 1221–1229 (1999).
112. Roche, S. & Gaudin, Y. Evidence that rabies virus forms different kinds of fusion machines with different pH thresholds for fusion. *J. Virol.* **78**, 8746–52 (2004).
113. de Duve, C. *et al.* Commentary. Lysosomotropic agents. *Biochem. Pharmacol.* **23**, 2495–531 (1974).
114. Al-Bari, M. A. A. Targeting endosomal acidification by chloroquine analogs as a promising strategy for the treatment of emerging viral diseases. *Pharmacol. Res. Perspect.* **5**, e00293 (2017).
115. Schuhmann, T. & Grond, S. Biosynthetic investigations of the V-type ATPase inhibitors bafilomycin A1, B1 and concanamycin A. *J. Antibiot. (Tokyo).* **57**, 655–61 (2004).
116. Whitbeck, J. C., Foo, C.-H., Ponce de Leon, M., Eisenberg, R. J. & Cohen, G. H. Vaccinia virus exhibits cell-type-dependent entry characteristics. *Virology* **385**, 383–91 (2009).
117. Laliberte, J. P., Weisberg, A. S. & Moss, B. The Membrane Fusion Step of Vaccinia Virus Entry Is Cooperatively Mediated by Multiple Viral Proteins and Host Cell Components. *PLoS Pathog.* **7**, e1002446 (2011).
118. Burkard, C. *et al.* Coronavirus Cell Entry Occurs through the Endo-/Lysosomal Pathway in a Proteolysis-Dependent Manner. *PLoS Pathog.* **10**, e1004502 (2014).
119. Georgi, A., Mottola-Hartshorn, C., Warner, A., Fields, B. & Chen, L. B. Detection of individual fluorescently labeled reovirions in living cells. *Proc. Natl. Acad. Sci. U. S. A.* **87**, 6579–83 (1990).
120. Stegmann, T., Morselt, H. W. M., Scholma, J. & Wilschut, J. Fusion of influenza virus in an intracellular acidic compartment measured by fluorescence dequenching. *Biochim. Biophys. Acta - Biomembr.* **904**, 165–170 (1987).
121. Tang, V. A., Renner, T. M., Fritzsche, A. K., Burger, D. & Langlois, M. A. Single-Particle Discrimination of Retroviruses from Extracellular Vesicles by Nanoscale Flow Cytometry. *Sci. Rep.* (2017). doi:10.1038/s41598-017-18227-8
122. Jayakar, H. R., Jeetendra, E. & Whitt, M. A. Rhabdovirus assembly and budding. *Virus Res.* **106**, 117–32 (2004).

123. Cureton, D. K., Massol, R. H., Whelan, S. P. J. & Kirchhausen, T. The length of vesicular stomatitis virus particles dictates a need for actin assembly during clathrin-dependent endocytosis. *PLoS Pathog.* (2010). doi:10.1371/journal.ppat.1001127
124. Ayala-Nuñez, N. V, Wilschut, J. & Smit, J. M. Monitoring virus entry into living cells using DiD-labeled dengue virus particles. *Methods* **55**, 137–43 (2011).
125. Wilson, J. M. *et al.* EEA1, a tethering protein of the early sorting endosome, shows a polarized distribution in hippocampal neurons, epithelial cells, and fibroblasts. *Mol. Biol. Cell* **11**, 2657–2671 (2000).
126. Vanlandingham, P. A. & Ceresa, B. P. Rab7 regulates late endocytic trafficking downstream of multivesicular body biogenesis and cargo sequestration. *J. Biol. Chem.* **284**, 12110–12124 (2009).
127. Cheng, X.-T. *et al.* Revisiting LAMP1 as a marker for degradative autophagy-lysosomal organelles in the nervous system. *Autophagy* **14**, 1472–1474 (2018).
128. Saha, D., Martuza, R. L. & Rabkin, S. D. Oncolytic herpes simplex virus immunovirotherapy in combination with immune checkpoint blockade to treat glioblastoma. *Immunotherapy* **10**, 779–786 (2018).
129. Walton, R. W., Brown, M. C., Sacco, M. T. & Gromeier, M. Engineered Oncolytic Poliovirus PVSRIPO Subverts MDA5-Dependent Innate Immune Responses in Cancer Cells. *J. Virol.* **92**, (2018).
130. Avilov, S. V. *et al.* Replication-Competent Influenza A Virus That Encodes a Split-Green Fluorescent Protein-Tagged PB2 Polymerase Subunit Allows Live-Cell Imaging of the Virus Life Cycle. *J. Virol.* **86**, 1433–1448 (2012).
131. Manini, I. *et al.* Role of microenvironment in glioma invasion: What we learned from in vitro models. *International Journal of Molecular Sciences* **19**, (2018).
132. Brown, N. F., Carter, T. J., Ottaviani, D. & Mulholland, P. Harnessing the immune system in glioblastoma. *Br. J. Cancer* **119**, 1171–1181 (2018).
133. Chen, Z. & Hambardzumyan, D. Immune microenvironment in glioblastoma subtypes. *Frontiers in Immunology* **9**, (2018).
134. Daniels, B. P. *et al.* Viral pathogen-associated molecular patterns regulate blood-brain barrier integrity via competing innate cytokine signals. *MBio* **5**, (2014).
135. Milora, K. A. & Rall, G. F. Interferon Control of Neurotropic Viral Infections. *Trends Immunol.* (2019). doi:10.1016/j.it.2019.07.005
136. Kreit, M. *et al.* Inefficient Type I Interferon-Mediated Antiviral Protection of Primary Mouse Neurons Is Associated with the Lack of Apolipoprotein L9 Expression. *J. Virol.* **88**, 3874–3884 (2014).
137. Cho, H. *et al.* Differential innate immune response programs in neuronal subtypes determine susceptibility to infection in the brain by positive-stranded RNA viruses. *Nat. Med.* **19**, 458–464 (2013).
138. Ida-Hosonuma, M. *et al.* The Alpha/Beta Interferon Response Controls Tissue Tropism and Pathogenicity of Poliovirus. *J. Virol.* **79**, 4460–4469 (2005).
139. Dietrich, J., Rao, K., Pastorino, S. & Kesari, S. Corticosteroids in brain cancer patients: benefits and pitfalls. *Expert Rev. Clin. Pharmacol.* **4**, 233–42 (2011).
140. Weathers, S.-P. & Gilbert, M. R. Current challenges in designing GBM trials for immunotherapy. *J. Neurooncol.* **123**, 331–7 (2015).
141. Desjardins, A. *et al.* Recurrent glioblastoma treated with recombinant poliovirus.

N. Engl. J. Med. **379**, 150–161 (2018).
142. Weidner, J. M. *et al.* Interferon-Induced Cell Membrane Proteins, IFITM3 and Tetherin, Inhibit Vesicular Stomatitis Virus Infection via Distinct Mechanisms. *J. Virol.* **84**, 12646–12657 (2010).
143. Han, Y. *et al.* Structure of human RNase L reveals the basis for regulated RNA decay in the IFN response. *Science* **343**, 1244–8 (2014).
144. Más, V. & Melero, J. A. Entry of enveloped viruses into host cells: Membrane fusion. *Subcell. Biochem.* **68**, 467–487 (2013).
145. Maletínská, L. *et al.* Human Glioblastoma Cell Lines: Levels of Low-Density Lipoprotein Receptor and Low-Density Lipoprotein Receptor-related Protein. *Cancer Res.* **60**, (2000).
146. Fan, Q. W., Iosbe, I., Asou, H., Yanagisawa, K. & Michikawa, M. Expression and regulation of apolipoprotein E receptors in the cells of the central nervous system in culture: A review. *J. Am. Aging Assoc.* **24**, 1–10 (2001).
147. Russell, L. & Peng, K. W. The emerging role of oncolytic virus therapy against cancer. *Chinese Clinical Oncology* **7**, (2018).
148. Lin, C. Z. *et al.* Advances in the mechanisms of action of cancer-targeting oncolytic viruses (review). *Oncology Letters* **15**, 4053–4060 (2018).
149. Howells, A., Marelli, G., Lemoine, N. R. & Wang, Y. Oncolytic viruses-interaction of virus and tumor cells in the battle to eliminate cancer. *Frontiers in Oncology* **7**, (2017).
150. Guo, D. *et al.* An LXR agonist promotes glioblastoma cell death through inhibition of an EGFR/AKT/SREBP-1/LDLR-dependent pathway. *Cancer Discov.* **1**, 442–56 (2011).
151. Jiang, L. *et al.* Combination of body mass index and oxidized low density lipoprotein receptor 1 in prognosis prediction of patients with squamous non-small cell lung cancer. *Oncotarget* **6**, 22072–22080 (2015).
152. Pedersen, N. B. *et al.* Low density lipoprotein receptor class A repeats are O-glycosylated in linker regions. *J. Biol. Chem.* **289**, 17312–17324 (2014).
153. Guibinga, G. H., Miyanohara, A., Esko, J. D. & Friedmann, T. Cell surface heparan sulfate is a receptor for attachment of envelope protein-free retrovirus-like particles and VSV-G pseudotyped MLV-derived retrovirus vectors to target cells. *Mol. Ther.* **5**, 538–546 (2002).
154. Schlegel, R., Tralka, T. S., Willingham, M. C. & Pastan, I. Inhibition of VSV binding and infectivity by phosphatidylserine: is phosphatidylserine a VSV-binding site? *Cell* **32**, 639–46 (1983).
155. Schloemer, R. H. & Wagner, R. R. Cellular adsorption function of the sialoglycoprotein of vesicular stomatitis virus and its neuraminic acid. *J. Virol.* **15**, 882–93 (1975).
156. Sun, X., Yau, V. K., Briggs, B. J. & Whittaker, G. R. Role of clathrin-mediated endocytosis during vesicular stomatitis virus entry into host cells. *Virology* **338**, 53–60 (2005).
157. van der Goot, F. G. & Gruenberg, J. Intra-endosomal membrane traffic. *Trends Cell Biol.* **16**, 514–21 (2006).
158. Sun, X., Roth, S. L., Bialecki, M. A. & Whittaker, G. R. Internalization and fusion mechanism of vesicular stomatitis virus and related rhabdoviruses. *Future*

Virology **5**, 85–96 (2010).
159. Sakata, M. *et al.* Analysis of VSV pseudotype virus infection mediated by rubella virus envelope proteins. *Sci. Rep.* **7**, (2017).
160. Brindley, M. A. & Maury, W. Endocytosis and a Low-pH Step Are Required for Productive Entry of Equine Infectious Anemia Virus. *J. Virol.* **79**, 14482–14488 (2005).
161. Laliberte, J. P., Weisberg, A. S. & Moss, B. The membrane fusion step of vaccinia virus entry is cooperatively mediated by multiple viral proteins and host cell components. *PLoS Pathog.* **7**, (2011).
162. Townsley, A. C., Weisberg, A. S., Wagenaar, T. R. & Moss, B. Vaccinia Virus Entry into Cells via a Low-pH-Dependent Endosomal Pathway. *J. Virol.* **80**, 8899–8908 (2006).
163. Gonçalves-Carneiro, D., McKeating, J. A. & Bailey, D. The Measles Virus Receptor SLAMF1 Can Mediate Particle Endocytosis. *J. Virol.* **91**, (2017).
164. Li, C. *et al.* The host restriction factor interferon-inducible transmembrane protein 3 inhibits vaccinia virus infection. *Front. Immunol.* **9**, (2018).
165. Suddala, K. C. *et al.* Interferon-induced transmembrane protein 3 blocks fusion of sensitive but not resistant viruses by partitioning into virus-carrying endosomes. *PLoS Pathog.* **15**, (2019).
166. Feeley, E. M. *et al.* IFITM3 inhibits influenza a virus infection by preventing cytosolic entry. *PLoS Pathog.* (2011). doi:10.1371/journal.ppat.1002337
167. Ibi, D. *et al.* Astroglial IFITM3 mediates neuronal impairments following neonatal immune challenge in mice. *Glia* **61**, 679–93 (2013).
168. Lagace, T. A. PCSK9 and LDLR degradation: Regulatory mechanisms in circulation and in cells. *Current Opinion in Lipidology* **25**, 387–393 (2014).
169. Kummer, S., Avinoam, O. & Kräusslich, H. G. IFITM3 clusters on virus containing endosomes and lysosomes early in the influenza a infection of human airway epithelial cells. *Viruses* **11**, (2019).
170. Georgel, P. *et al.* Vesicular stomatitis virus glycoprotein G activates a specific antiviral Toll-like receptor 4-dependent pathway. *Virology* **362**, 304–313 (2007).
171. Rallabhandi, P. *et al.* Respiratory syncytial virus fusion protein-induced toll-like receptor 4 (TLR4) signaling is inhibited by the TLR4 antagonists Rhodobacter sphaeroides lipopolysaccharide and eritoran (E5564) and requires direct interaction with MD-2. *MBio* **3**, (2012).
172. Blasius, A. L. & Beutler, B. Intracellular Toll-like Receptors. *Immunity* **32**, 305–315 (2010).
173. Wang, J. P. *et al.* Flavivirus activation of plasmacytoid dendritic cells delineates key elements of TLR7 signaling beyond endosomal recognition. *J. Immunol.* **177**, 7114–21 (2006).
174. Furr, S. R., Moerdyk-Schauwecker, M., Grdzelishvili, V. Z. & Marriott, I. RIG-I mediates nonsegmented negative-sense RNA virus-induced inflammatory immune responses of primary human astrocytes. *Glia* **58**, 1620–9 (2010).
175. Huang, J. *et al.* Inhibition of type I and type III interferons by a secreted glycoprotein from Yaba-like disease virus. *Proc. Natl. Acad. Sci. U. S. A.* **104**, 9822–9827 (2007).
176. Dilley, K. A. *et al.* The Ebola virus VP35 protein binds viral immunostimulatory and

host RNAs identified through deep sequencing. *PLoS One* **12**, (2017).
177. Lindqvist, R., Kurhade, C., Gilthorpe, J. D. & Överby, A. K. Cell-type- and region-specific restriction of neurotropic flavivirus infection by viperin. *J. Neuroinflammation* **15**, 80 (2018).
178. Liu, J. *et al.* A synthetic double-stranded RNA, poly I:C, induces a rapid apoptosis of human CD34(+) cells. *Exp. Hematol.* **40**, 330–41 (2012).

CONTRIBUTIONS OF COLLABORATORS

The neurotoxicity of FMT-(MRB-G) and MRB-(FMT-G) *in vivo* experiment was performed by Beta Yadollahi in Dr. Stojdl's lab at the CHEO Research Institute II. All rhabdoviruses used in this study were developed by Charles Lefebvre and Melanie Labelle in Dr. Stojdl's lab, and the vaccinia virus stocks were generated by Kristina Allan in Dr. Stojdl's lab as well. Phil Charron in Dr. Stojdl's lab assisted me in writing the R script and performed the qPCR titration of my viral stocks for the viral binding experiment. Matteo Da Ros from Turnstone Biologics performed the viral RNA extraction for the qPCR titration of the viral stocks. Corina Stewart and Dr. Marceline Côté's from the University of Ottawa kindly provided me with endosome acidification drug inhibitors to test for my experiments. Skye McBride and Chloe Van Oostende Triplet assisted with the design of the lipid mixing assay imaging experiment. Tyler Renner from Dr. Langlois' lab at the University of Ottawa taught me how to indirectly label viruses with DiD.

APPENDIX

Supplementary Figures

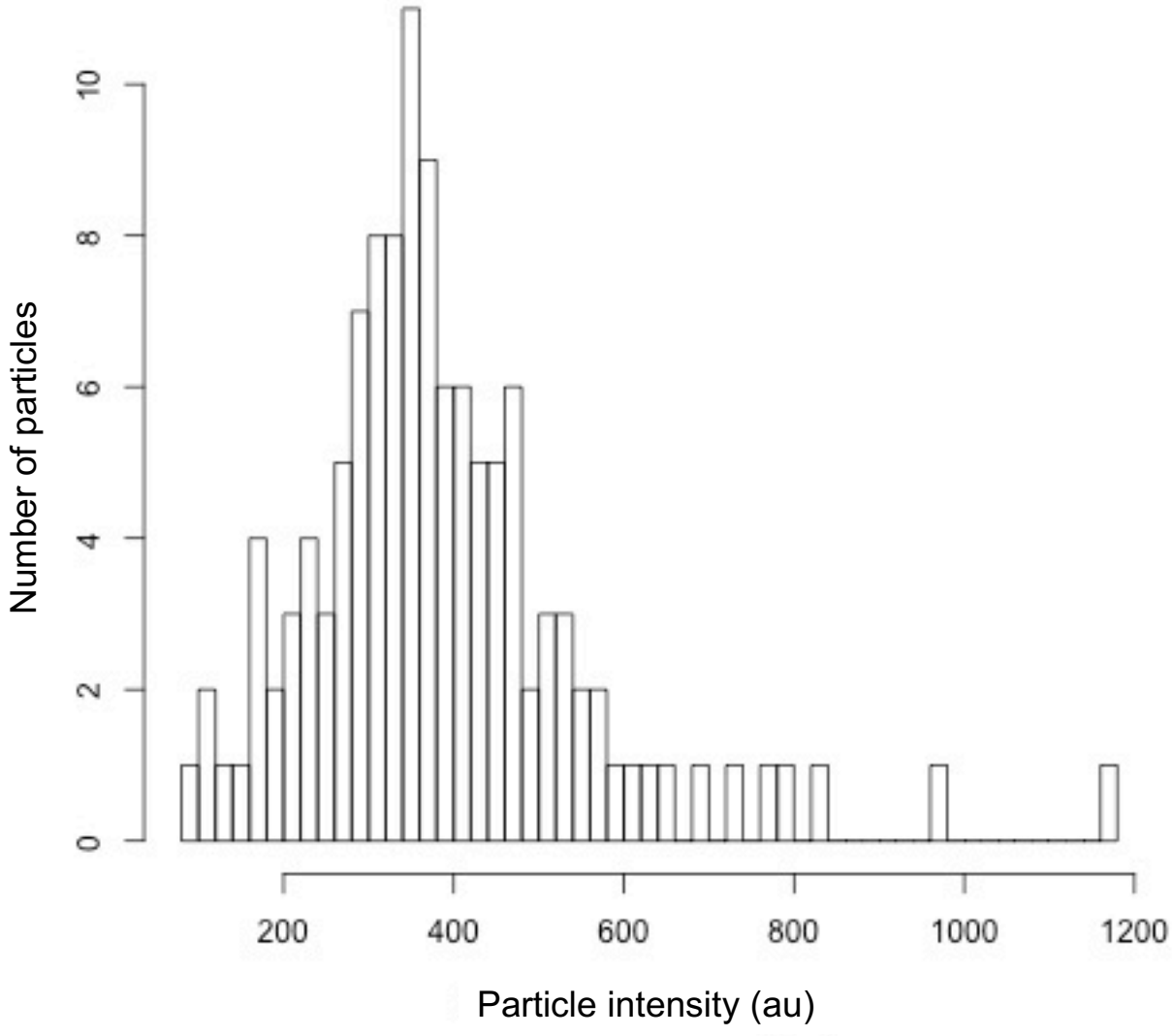

Figure S1. Fluorescence intensity of DiD-labeled FMT particles. FMT was indirectly labeled with DiD dye then bound to U343 cells stained with DAPI. Cells were imaged via confocal microscopy in the Alexa-647 and DAPI channels. Particle intensities were quantified via ImageJ analysis.

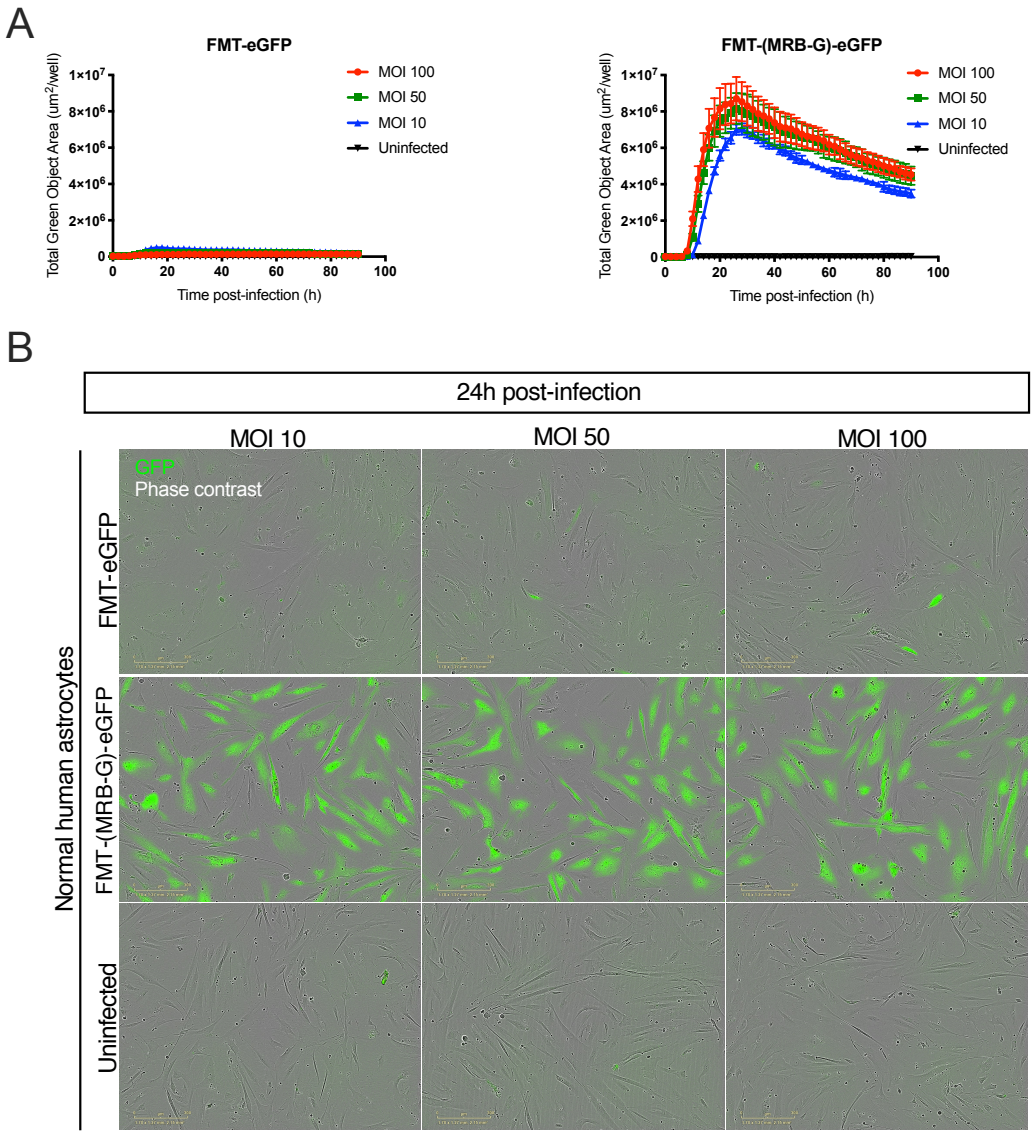

Figure S2. FMT-eGFP and FMT-(MRB-G)-eGFP infection at high MOIs in normal human astrocytes. (A) NHA cells were infected with FMT-eGFP or FMT-(MRB-G)-eGFP at MOI 10, 50, or 100. Total GFP fluorescence from infected cells was monitored in real time using IncuCyte live cell imaging for a total of 90 hours. N = 3 technical replicates. Data in all figures represents group means +/- SD. (C) A panel of representative images show overlay phase contrast and GFP fluorescence microscopy images of the infected NHA cells at 24 hours post-infection.